Laboratory of Molecular Science and Engineering

Faculty of Science and Engineering

Åbo Akademi University

Analytical Chemistry Group

Laboratory of Environmental Chemistry

Paul Scherrer Institute

ANALYSIS OF MAJOR IONS, STABLE WATER ISOTOPES AND BLACK CARBON IN THE UPPER PART OF BELUKHA ICE CORE, SIBERIAN ALTAI

Viola Wilson

Master's thesis in chemistry carried out under the supervision of Prof. Dr. Margit Schwikowski-Gigar, Dr. Rose-Marie Latonen and Assoc. Prof. Tom Lindfors

August 2020 – May 2021

ABSTRACT

There are many different paleoarchives, e.g. sediments, ice cores, tree-rings, speleothems and corals. This master's thesis focuses on the information receivable from ice cores. Well preserved information of past precipitation can be found as natural archives in glaciers. This is possible if the melting is negligible and if the precipitation during the year occurs as snow. Annual snow layers will contain information of chemical impurities and stable water isotopes, which can determine past climate and air pollution. Climate change reduces the volume of glaciers all around the world, it is therefore important to conduct paleoclimatic research and retrieve ice cores while the opportunity still exists.

Concentrations of major ions, and Black Carbon (*BC*) as well as the ratio of stable isotopes of oxygen and hydrogen in water were analyzed for the first 26.5 m of an ice core from the Belukha glacier in the Siberian Altai. Some melting had occurred on the glacier, which led to shifting or loss of some chemical signals. Clear signals for mineral dust-related species (calcium, magnesium, sodium and chloride), anthropogenic-related species (nitrate, sulphate and ammonium) and the biogenic and biomass burning related species (formate, oxalate and ammonium) could still be seen. The dating was accomplished by comparing the records with another ice core drilled from the Belukha glacier in 2001. One distinct dust peak and seasonally varying signals proved to be significant for dating. This part of the ice core extended back to year 1984 and a good agreement could be made between the two ice cores from Belukha. Most of the analyzed ions showed a decreasing trend in concentration from 1984 to 2018. An exception was the concentrations for methanesulfonic acid (*MSA*) and potassium. The increase in MSA (sea-ice proxy) was believed to be due to melting of ice in the Arctic Ocean. The increase in potassium concentrations was not easily explained.

The mean $\delta^{18}O$ value (-13.09‰) was considered a high value for the elevation of 4506 m a.s.l., this indicated lack of strong winter minima. The deuterium-excess (*d-excess*) value was higher during the winter months and lower during the summer months, which suggested an input of water vapor from internal sources during the winter and from external sources during the summer. One dust layer was visually observed in the ice core; this dust event happened in 2006 and the increased calcium and magnesium concentration at this depth confirmed the dust event.

Key words: Air pollution, Climate reconstruction, Ice core analysis, Stable water isotopes, Major ions, Black carbon, Belukha.

ABBREVIATIONS

APD	Avalanche Photodiodes
B01	Belukha Ice Core 2001
B18	Belukha Ice Core 2018
BC	Black Carbon
d-excess	Deuterium Excess
DMS	Dimethyl Sulfide
DOC	Dissolved Organic Carbon
FSU	Former Soviet Union
IAEA	International Atomic Energy Agency
IC	Ion Chromatography
ICP-MS	Inductively Coupled Plasma – Mass Spectrometry
LOD	Limits of Detection
MSA	Methanesulfonic Acid
OC	Organic Carbon
WS-CRDIS	Wavelength-Scanned Cavity Ring-Down Infrared Spectroscopy
PET	Polyethylenterephthalate
POC	Particulate Organic Carbon
PSI	Paul Scherrer Institute
rBC	refractory Black Carbon
SMOW	Standard Mean Ocean Water
SP2	Single Particle Soot Photometer
SWI	Stable Water Isotopes

TABLE OF CONTENTS

1 INTRODUCTION

The cryosphere, i.e., glaciers, snow, permafrost and other ice, covers 10% of the Earth's surface. Glaciers are built up by deposition of countless layers of snow over a period of thousands of years. These glaciers are a unique source of information about past atmospheric conditions. Ice cores drilled from glaciers are excellent archives for understanding the past environmental and climatic changes. Different information can be obtained, depending on the location of the glacier. Polar ice cores, e.g. those extracted from Antarctica and Greenland, contain information at a global scale, whereas ice cores from low- and mid-latitudes, e.g. the European Alps and the Asian High Mountains, contain information about the local climate. Possible information that can be extracted from polar ice cores are e.g. signals of past temperatures, greenhouse gases, precipitation and concentration of aerosols. The focus in this thesis will be on the low- and mid-latitude glaciers, not on the polar ice. Advantages with the low- and mid-latitude glaciers are that they show more precise records of local climate, which is important since a large part of the Earth´s population lives in these regions. It is also possible to extract information about the variations of the climate from both anthropogenic and natural factors from these glaciers. Industries and cities often emit short-lived atmospheric species, which can be extracted from low- and mid-latitude glaciers. The precipitation is usually high in these regions, which establishes records with high resolution. The low- and mid-latitudes also enable analysis of meteorological processes, e.g., by analyzing the dust depositions from different deserts (Garzonio, et al., 2017).

It is important to analyze glaciers when the opportunity still exists. The recent global warming has led to retreatment of low- and mid-latitude glaciers. It is estimated that 80% of the glacier mass of smaller glaciers in, e.g., the European Alps and North Asia, will be melted by year 2100. This estimation is made under the warming scenario called RCP8.5, which is the estimated scenario if no efforts to cut greenhouse gas emissions are made (IPCC, 2019). Melting of glaciers will make it impossible to obtain important paleoclimatic records. The melting of glaciers is causing us to lose a part of our planet's history (Fig. 1.). It is, therefore, urgent for us to preserve as many ice cores as possible from selected glaciers around the world. The global warming sets a strict race against the time to collect ice cores from endangered glaciers. To act on this emergency the Ice Memory project was created. The goal for this international project is to create a global ice archive sanctuary for ice core records recovered from all around the world. The ice cores will be stored in a perennial subsurface

storage space in Antarctica. The ice cores will be saved for future generations to analyze (Bronex, et al., 2020; Ice Memory, 2020). The biomass, peatlands and soil in Siberia are one of the largest reservoirs of terrestrial carbon in the world (Olivier, et al., 2006). The estimated temperature increase for northern Asia within the current climate change scenario (IPCC, 2014), poses a major threat. Massive amounts of terrestrial carbon could be released by forest fires due to increased temperature.

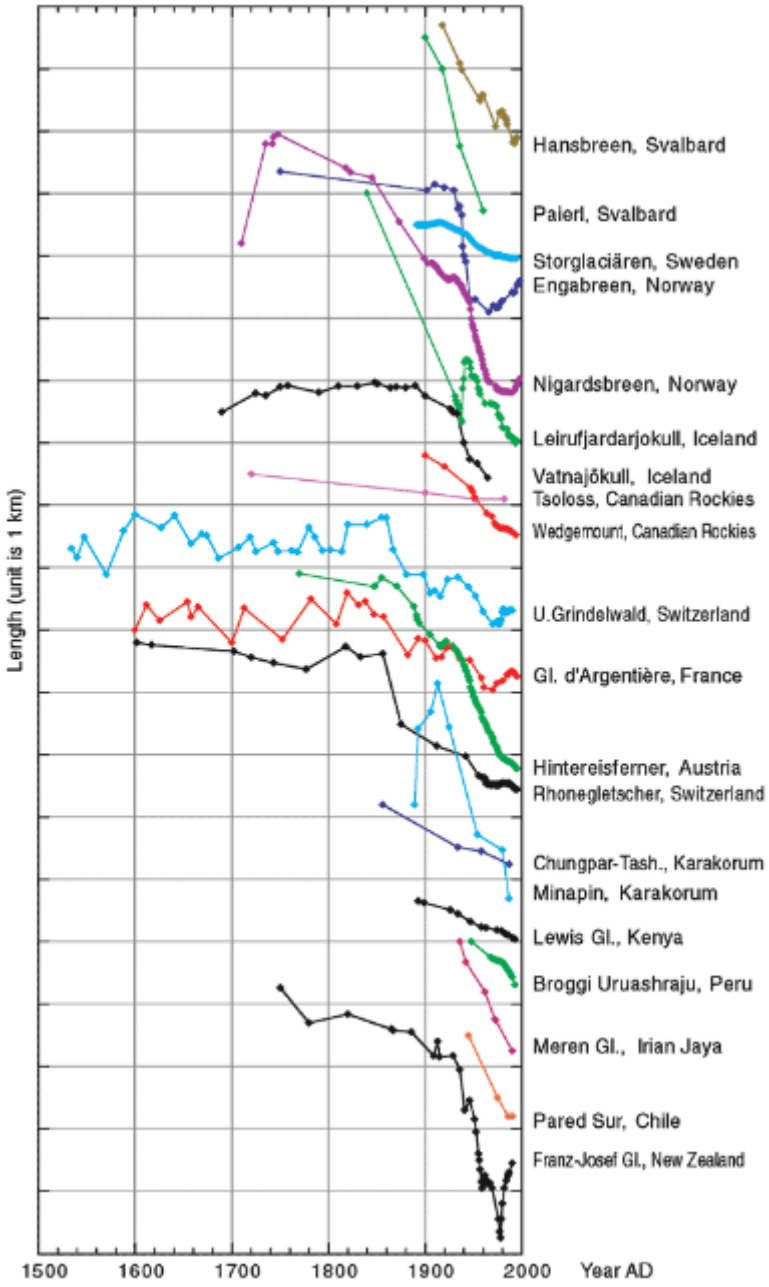

Fig. 1. The length of twenty different glaciers around the world. The curves are translated to the vertical axis for easier comparison, figure from (IPCC, 2001).

2 BACKGROUND

2.1 Stable water isotopes

The Danish paleoclimatologist Willi Dansgaard (1922 – 2011) discovered that past temperatures could be reconstructed by analyzing stable isotopes of oxygen and hydrogen found in glaciers (Rapp, 2012). There are three naturally occurring stable isotopes of oxygen (^{16}O, ^{17}O and ^{18}O) and two naturally occurring stable isotopes of hydrogen (^{1}H and D). This leads to four different isotopologues of water, i.e. molecules with varying isotopic composition. The light isotopologue $H_2{}^{16}O$ is the most abundant isotopologue, the heavier isotopologues are $H_1D^{16}O$, $H_2{}^{17}O$ and $H_2{}^{18}O$. These isotopologues of water are with a common name called stable water isotopes (*SWI*). Two of these SWI, $H_2{}^{18}O$ and $HD^{16}O$, are naturally occurring tracers and used in paleoclimatology research (Beria, et al., 2018). The use of ^{17}O as a natural tracer has increased recently (Landais, et al., 2008); however, ^{17}O is not considered further, since it was not used as a tracer in this research. In the past, SWI ($H_2{}^{18}O$ and $HD^{16}O$) were expressed as ppm, but they are now expressed as δ notation with the unit per mil (‰). The isotopic composition of water can be determined with the help of the international standard reference, i.e. the Standard Mean Ocean Water (*SMOW*). The reference value is provided by the International Atomic Energy Agency (*IAEA*). The isotopic composition is expressed as delta notation (*δ*), which is the deviation from the ratio (*R*) of $^{18}O/^{16}O$ or $D/^{1}H$ of a sample from the standard reference SMOW (see Equation 1.) (Rapp, 2012).

$$\boldsymbol{\delta^{18}O \text{ or } \delta D} \ (‰) = \frac{\boldsymbol{R\ sample - R\ standard}}{\boldsymbol{R\ standard}} \boldsymbol{x\ 1{,}000}$$

Equation 1. The definition of $\delta^{18}O$ and δD is shown. R sample represents the $^{18}O/^{16}O$ fractionation for $\delta^{18}O$ and D/H fractionation for δD. R standard represents the SMOW value.

2.2 Isotopic fractionation

Isotopic fractionation occurs during each phase change, i.e. stable isotopes are enriched in one phase and depleted in another. The two mass-dependent effects that influence the fractionation behavior of the SWI are called the equilibrium effects. The diffusion velocity is slower for the heavier isotopologues, because of the heavier weight. The heavier isotopologues prefer phases with stronger bonds (solid > liquid > vapor), because of the larger mass. The evaporated water will have a lower $\delta^{18}O$-value, i.e. will be depleted in

heavier isotopologues, since they have a lower tendency to evaporate. The air parcel cools down when it moves towards the pole (Fig. 2.). When the air parcel reaches the Dew point, it will start to condensate. This means that the $\delta^{18}O$-value of the air parcel will decrease further when it becomes colder and more water will condensate out of it. The temperature can be determined from the $\delta^{18}O$ or the δD, since the magnitude of the enrichment of heavier isotopes is temperature dependent. Precipitation during warmer periods (summer) is less depleted compared to precipitation during colder periods (Rapp, 2012).

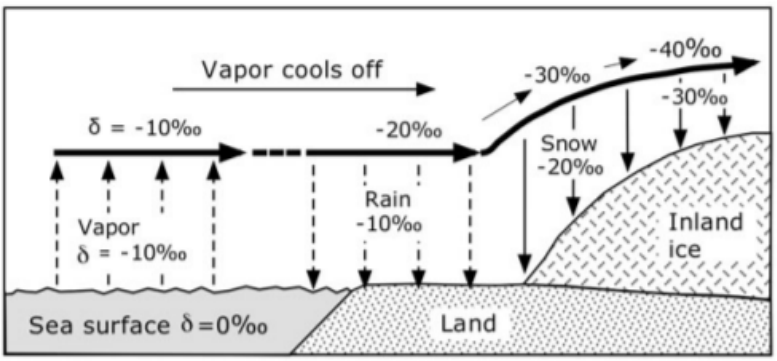

Fig. 2. Isotopic fractionation, δ-values for different reservoirs, figure from (Rapp, 2012).

The deuterium excess (*d-excess*) is used to identify the precipitation source regions. Most of the global precipitation originates from the oceans. Some of the moisture in the atmosphere is recycled from other sources than the ocean. Water can evaporate from lakes and soils, but also from plant transpiration. The relative mass difference of the hydrogen isotopes is eight times bigger than the relative mass difference of the oxygen isotopes. That is why $\delta^{18}O$ is multiplied by eight (see Equation 2.). The d-excess is the deviation of a water sample from the global meteoric water line. The d-excess is affected by the isotopic fractionation at the evaporation source and it correlates with the temperature and relative humidity.

$$d - excess = \delta D - 8\ x\ \delta^{18}O$$

Equation 2. The definition of *d*-excess, the δD value subtracted from eight multiplied with the $\delta^{18}O$ values.

2.3 Glaciers as natural archives

The transition from snow to ice, i.e. dry snow metamorphosis, occurs due to mechanical packing and plastic deformation. The density increases when more snow accumulates on the surface and the material becomes more compressed. The compression forces the snow to recrystallize and form grains. With time, these grains become similar in size and larger. At a certain depth below surface, e.g. at around 50 m depth for high-altitude glaciers, the so-

called firn grains sinter and form glacier ice, which is not porous anymore. Year by year snow accumulation is added in the accumulation area of the glacier, which turns into distinct layers. For this to be possible, the yearly precipitation needs to be snow and melting needs to be negligible. These conditions can usually be found at high elevations, around 4000 m a.s.l. (Rapp, 2012).

Much information can be obtained from the ice, it is a unique archive of paleo-atmospheric conditions and paleoclimate. Information about atmospheric composition, solar activity, volcanism, biomass burning, dustiness and past temperatures can be obtained (Rapp, 2012). Trace species can also be determined, they originate from natural or anthropogenic sources. The natural sources include sea spray, volcanic eruptions and mineral dust. The anthropogenic sources include agriculture, energy production, traffic and fossil fuel combustion (Schwikowski, et al., 2010). Some species can be used as tracers for a specific source; chloride and sodium from sea salt, calcium and magnesium from dust, sulphate, nitrate and ammonium from anthropogenic sources, ammonium and formate from biomass burning. The oldest ice core ever retrieved is 2.7 million years old from Allan Hills, Antarctica. This ice core contains information about the Earth's atmosphere from when the ice age began. The Allan Hills is near the coast, where the glacial flow brings older ice to the surface. The oldest ice core drilled from the mainland of Antarctica (Dome C) is ~800,000 years old. This core contained a continuous record, in contrast to the one from Allan Hills which just gave access to an old, but short time scale. The deepest part of the ice cores from the mainland can be affected by melt due to heat from the bedrock (Voosen, 2017).

Among the trace species, BC particles have received a lot of attention recently. They are formed by incomplete combustion of carbonaceous matter, i.e. biomass and fossil fuel. Due to their unique properties, i.e. low chemical activity, strongly light-absorbing and highly refractory, BC particles affect the Earth's radiative budget. BC contributes to the global warming by reducing the albedo of snow, directly absorbing sunlight in the atmosphere and modifying cloud properties (Osmont, et al., 2018). Greenhouse gases are the largest contributor to global warming, but BC is believed to be the second largest (Dutkiewicz, et al., 2014). The European Union was among the first which worked to reduce emission of air pollutants. Studies have shown that BC particles can cause health problems, e.g. respiratory and cardiovascular diseases. BC particles can also introduce toxins, e.g., heavy metals and polycyclic aromatic hydrocarbons into the human body, since they operate as universal carriers (Sun, et al., 2020). It is highly important to study BC records from ice cores to better

understand the role BC particles play in the atmosphere. The recommendation to use the term rBC (*refractory black carbon*) for samples analyzed with laser-induced incandescence will hereafter be followed (Petzold, et al., 2013).

2.4 Ice core dating

Ice cores contain much information about the past climate, but without the age knowledge at each depth, the information has little value. To establish the most accurate age knowledge of an ice core, a combination of several different techniques is usually used. The uncertainty of the dating increases with the age of the ice core, i.e. the accuracy for recent periods is very good but becomes more uncertain further back in time. The determination of the timescale can become difficult if irregular deposition of precipitation occurs. The appropriate dating method used for ice cores depends on the accuracy requirements and on the length (i.e. age) of the ice core (Eichler, et al., 2000).

2.4.1 Seasonally varying signals

Dating with seasonally varying signals for ice cores is a very precise method, the principle is the same as counting annual rings on trees. The annual layers in ice cores can be up to several meters at the top but only a few centimeters further down in the ice core. The annual signals can be more difficult to identify further down in the glacier, due to layer thinning. Annual layers become thinner with depth, due to gravity that causes the ice to flow from the accumulation area to the ablation zones. The bedrock causes shearing and folding of the ice, which can lead to stratigraphic disturbance of the layers. The thinning of the ice and the stratigraphic disturbance must be considered when dating an ice core (Rapp, 2012).

One example of a seasonally varying signal is the isotopic ratio $^{18}O/^{16}O$ of water. This isotopic ratio is dependent on the condensation temperature, which is seasonally dependent. This hydrological cycle causes higher $\delta^{18}O$ values during summer precipitation and vice versa for winter precipitation. Another good seasonally varying signal is the ammonium concentration. This is one of the analyzed ions that show the most pronounced seasonal variations. The concentration for NH_4^+ is significantly higher in precipitation during summer months. This is because the precursor for NH_4^+ is NH_3, which is mainly emitted during summer months from agricultural emissions (90%), i.e. fertilizers and livestock excreta. The vertical transport of air masses and pollutants from emission sources to high altitudes is significantly larger during summer months (Eichler, et al., 2000).

2.4.2 Radioactive decay

Ice cores can be dated with environmental radionuclides, an example of which is ^{210}Pb dating. It was G. Cozaz in the early 1960s who first used ^{210}Pb to date ice cores. The most abundant isotope of uranium is ^{238}U, which is found at a level of ~ 1.7 ppm in the Earth's continental crust. ^{238}U (half-life 4.6 x 10^9 years) decays into the ^{226}Ra (half-life 1622 years) which, in turn, decays into the short-lived radioactive isotope ^{222}Rn, which is a noble gas (half-life 3.8 days). This gas is emanated from the soil into the atmosphere, where transportation in the lower troposphere occurs. ^{222}Rn decays to several short-lived heavy metal intermediate nuclides (half-life less than 30 min) that attach to aerosols in the atmosphere. Thereafter is the radio nuclide ^{210}Pb formed (half-life 22.3 years), which usually remains around two weeks in the atmosphere before deposition on the Earth's surface, e.g., on a glacier with precipitation. ^{210}Pb decays via the short-lived intermediate nuclides ^{210}Bi (half-life 5 days) and ^{210}Po (half-life 138 days) to the stable end product of the ^{238}U decay chain ^{206}Pb (Fig. 3). ^{210}Pb in ice can be measured via the decay of ^{210}Po, and since the concentration of ^{210}Pb in the air is well monitored, it can be used to determine age-depth scale for the ice core. The maximum dating time range is determined from the radioactive isotope ^{210}Pb half-life, the accessibility is $\sim$150 years (Gäggeler, et al., 2020).

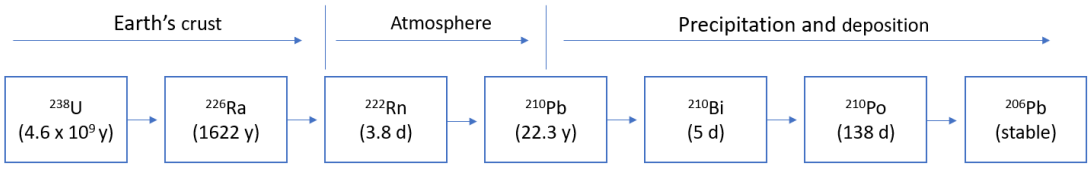

Fig. 3. Overview of the ^{238}U-^{206}Pb decay chain, modified from (Gäggeler, et al., 2017).

For this dating method, some assumptions need to be taken into consideration. The concentration of ^{210}Pb in precipitation is believed to be constant during the investigated timeline. Melting of the ice does not transport the ^{210}Pb containing particles in the ice. The concentration of ^{226}Ra in the ice is negligible and no additional ^{222}Rn diffuses from the atmosphere to the glacier (Gäggeler, et al., 2017).

2.4.3 Stratigraphic markers

Stratigraphic markers contain unusually high concentrations of debris in ice cores at certain depths (i.e., a known age). The debris originates from well-known events, creating so-called reference horizons. Reference horizons can originate from increased concentration of pollutants from e.g., forest fires, desert dust, anthropogenic factors and volcanic eruptions

(Eichler, et al., 2000). Examples of some well-known reference horizons are increased sulphate concentrations in the ice due to the Mount Katmai volcanic eruption in Alaska in 1912 and the Tambora volcanic eruption in Indonesia in 1815/1816 (Henderson, et al., 2006). Another example is the varying sulfur dioxide emissions in Kazakhstan and Siberia. A sharp increase in sulphate concentration can be seen in the 1970s followed by a decrease in the 1980s due to political and economic crises when coal was replaced with gas. In the 1950s, an increase in ammonium concentration is seen because of the population inflow in southern Siberia (increased agricultural activity). The increased use of fertilizers and traffic growth is noticeable as an increase in the nitrate concentrations starting from the 1960s. The last example is the nitrate peak in 1908 from the mysterious Tunguska event in Russia (Olivier, et al., 2006).

Radioactive debris from certain events is commonly used as reference horizons. One example is the Chernobyl nuclear reactor accident in 1986 and the nuclear weapon testing in the 1950s and 1960s, all of which released huge amounts of ^{137}Cs into the atmosphere. ^{137}Cs is a long-lived radioactive isotope originating from nuclear reaction. This radioactive isotope and other nuclear debris can be absorbed onto aerosol particles and, therefore, be detected in ice cores. Tritium (^{3}H) exists naturally in the atmosphere, but in a much lower concentration compared to hydrogen and deuterium. ^{3}H is produced naturally in the atmosphere in a reaction with oxygen, nitrogen and high-energy cosmic rays. It reacts with water molecules in the atmosphere and reaches the glaciers as precipitation. There are, however, anthropogenic origins for ^{3}H as well. Anthropogenic ^{3}H was released with the world's first thermonuclear explosion in 1951. The concentration of ^{3}H increased until the Test Ban Treaty was signed in 1963 by the Soviet Union and the United States. The ^{3}H peak in 1963 is commonly used as a stratigraphic marker in ice core dating (Eichler, et al., 2000).

2.5 Altai Mountains

The site selection for obtainment of ice cores from mid- and low-latitude glacier is important. To obtain interpretable records, some important criteria need to be fulfilled when choosing a suitable glacier. It is important to consider the climatic variables on the site, e.g. wind exposure and accumulation rate, when choosing a suitable drilling site. The glacial thickness needs to be sufficient to ensure long-term records. The glacial thickness depends on the input of annual snow accumulation but also on the snow output due to wind erosion. One also needs to consider the physical and morphological features on the site, e.g. melting, and flow

velocity. Glacial flow can lead to disruptions in annual layers; relatively flat surface topography is therefore optimal. To minimize disruptions of meltwater percolations high elevation sites can be used. One last consideration is the accessibility of the site, usually above 4 000 m a.s.l. (Garzonio, et al., 2017).

Relatively few paleo-climatic records have to this date been obtained from the Altai Mountains. The paleo-climatic information obtained from the Altai is, however, of much interest. It is the location of the Altai Mountains that makes them interesting for paleoclimatology research. This location demonstrates a high degree in continentality, with high seasonal temperature variations from, -47 °C in winter to +41 °C in summer. It is located in Central Asia in the north-western periphery on the boarders between China, Kazakhstan, Mongolia and Russia (Fig. 4.). The Altai Mountain range extends from the Russian Altai in the north-west to the Gobi Desert in the south-east. The rivers Irtysh, Yenisei and Ob receive their main water input from the Altai mountain range. The Altai massif is 1500 km long and varies from 600 to 100 km from north to south. Belukha Mountain (4 506 m a.s.l.) is the highest peak in the Altai Mountains (Malygina, et al., 2017).

The snow accumulation in the Altai region derives mainly from an external marine source (67%), the rest derives from an internal moisture source. The main marine source is the Atlantic Ocean (56%), from where moisture is evaporated and transported with the Westerlies to the Altai region. The internal source is Central Asia, which is a major precipitation source during summer. The snow accumulation rate is higher during summer for both internal and external moisture sources. The air transport is prevented by the Siberian High during the winter, when the conditions are dry and cold. (Aizen, et al., 2006). The Altai Mountain functions as a barrier, which creates a north-west to south-east precipitation gradient. The annual precipitation on the north-west side is 400 to 600 mm, whereas the annual precipitation on the south-east side is ∼100 mm (Klinge, et al., 2003).

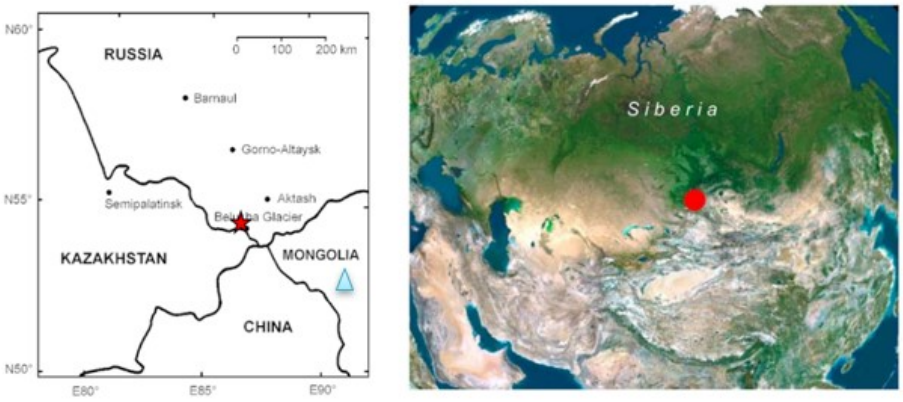

Fig. 4. On the left side, Belukha glacier is marked with a red star and Tsambagarav glacier with a blue triangle. On the right side, Altai Mountains is marked with a red dot. It can also be seen that the Altai Mountains is in-between the arid region of Central Asia and the vast Siberian forest (Eichler, et al., 2009b).

2.5.1 Belukha ice core 2001

Previous paleoclimatology research has been conducted by Paul Scherrer Institute (*PSI*) in the Siberian Altai. The first deep ice core drilled from the Belukha glacier in the Siberian Altai (4062 m a.s.l., 49°48'26.3''N, 86°34'42.8''E), by PSI, was drilled in July 2001 (Olivier, et al., 2006). The recovered ice core was 139 m long and a total of 3615 samples were obtained. The retraceable period covered by the ice core extended to 1250 AD. The inner part of the ice core was used to analyze the following cations Na^+, NH_4^+, K^+, Ca^{2+}, Mg^{2+} and the following anions Cl^-, NO_3^-, SO_4^{2-}, $HCOO^-$. The outer part of the ice core was used for ^3H, ^{210}Pb and $\delta^{18}O$ analyses. ^3H and ^{210}Pb were used to date the ice core and $\delta^{18}O$ for determining the amount of precipitation and temperature. The average $\delta^{18}O$ value was 12%, which is considered relatively high. The mean annual accumulation rate was calculated to be 0.56 m water equivalent (w. eq.) (Eichler, et al., 2009a). A back-trajectory analysis for the air transport to the Altai region during summer shows from where the air pollution originates. In the back-trajectories for the summer months of 1991 to 2000, it can be seen that the territory of the Former Soviet Union (*FSU*) is the main area of origin (Fig. 5.). Despite the remoteness of the Belukha Mountain, traces of anthropogenic impacts were seen in the form of ammonium, sulfate and nitrate. Differences in the ion concentration between Belukha and the Swiss Alps could be seen for ammonium and formate. This indicated enhanced concentrations from biogenic emissions from the Siberian forest. Ice lenses up to 20 cm thickness were observed, which indicated melting and refreezing during warm periods (Olivier, et al., 2019).

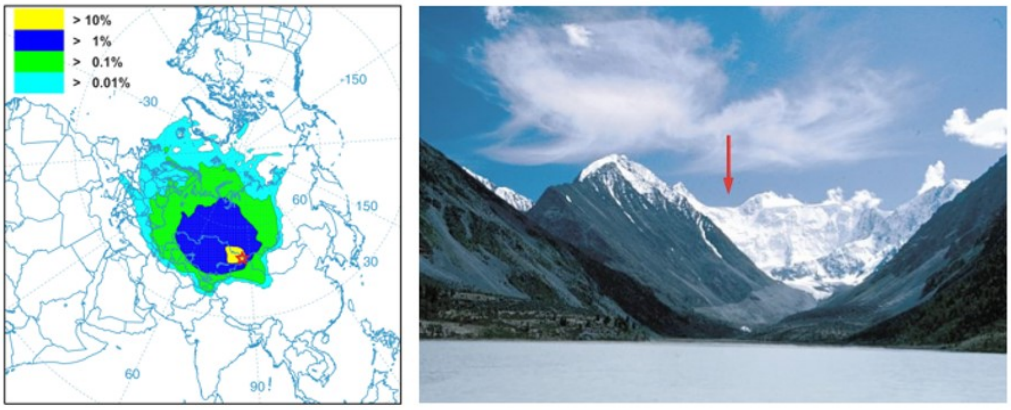

Fig. 5. To the left is a back-trajectory map of atmospheric transport in the Altai region (Eichler, et al., 2009b). To the right is the Belukha Mountain seen from the Ak-kem lake, photograph taken by Patrick Ginot. Both ice cores, the one drilled in 2001 and the one drilled in 2018, were recovered from the saddle between the east and west summit (49°48'N, 86°34'E) (Eichler, et al., 2009c).

2.5.2 Reason for drilling B18

Some questions where left unanswered when the Belukha ice core 2001 (*B01*) was analyzed. One of the questions left was the recent development of former Soviet Union (FSU) heavy metal emissions. Heavy metals pollute the atmosphere, particularly Pb, which can have devastating effects on human health. Pb pollution is worldwide quite well documented, however, some controversy can be seen regarding the existing Pb records for the FSU. Official reports by HELCOM (intergovernmental organization) estimate a decrease in the Pb emission for the period 1990 to 2007 (Gusev, 2009). An increase of the Pb concentrations during the 1990s was seen in an ice core obtained from the Tian Shen. Tian Shen is a mountain range also located in central Asia and this ice core is strongly influenced by emissions from China and FSU (Grigholm, et al., 2016). Because of the location of the Belukha glacier, the ice core can be used to study the recent changes in metal pollution from FSU. B18 will also be used to reconstruct the pre-industrial to industrial changes of organic aerosols. Atmospheric aerosols affect the climate directly and indirectly: directly by absorbing and scattering the radiation and indirectly by acting as cloud condensation nuclei, which affects the outgoing and incoming solar radiation. The effect aerosols have on the climate is still poorly understood, mainly because of the lack of knowledge about the number of particles in the natural atmosphere before the high increase due to anthropogenic pollution.

2.5.3 Acquisition of Belukha ice core 2018

The second expedition to Belukha took place in May – June 2018. The equipment was brought up with the help of a helicopter. The thickness of the glacier at the drilling site was already determined in 2001, this was done with the help of a radar. The radar signal penetrates through the ice and is reflected back to the surface by the bedrock. The ice cores were collected using an electromechanical ice core drill. The drill itself is 257 cm long and attached to a 200 m long cable. The ice cores were obtained as cylinders with a diameter ∼8 cm and length ∼70 cm. The drilling at the first site had to stop at a depth of 109 m, because no drilling chips were seen, suggesting the presence of a subsurface crevasse. The drill was packed up and reassembled at another location (49°48'27.7''N, 86°34'46.5''E, 4055 m asl.), where the second ice core was drilled. This time the bedrock was reached, at a depth of 163 m. The ice cores were carefully put in polyethylene tubes, labelled and put in cardboard boxes with styrofoam insulation. The ice cores filled up 21 cardboard boxes, which were transported in a frozen condition to Switzerland. The ice cores were stored in a freezer facility in Möhlin, Switzerland, due to limited space at the cold room at PSI.

3 AIM OF THIS WORK

As previously mentioned, research has already been conducted on ice cores from the Belukha glacier in the Siberian Altai. This master's thesis is based on a ten-week internship at PSI. The internship was involved with the ongoing research of the Belukha ice core drilled in 2018. The aim of this internship and therefore also of this master's thesis, was to learn how information about past air temperature, atmospheric composition, precipitation and wind pattern can be obtained from ice cores.

To achieve this, the upper part of the Belukha ice core was analyzed with the following methods, Single Particle Soot Photometer (*SP2*), Wavelength-Scanned Cavity Ring – Down Infrared Spectroscopy (*WS - CRDIS*) and ion chromatography (*IC*). SP2 was used to analyze black carbon concentration, WS – CRDIS was used to analyze SWI and IC was used to analyze ion concentrations. Before these analyses could begin, the ice core needed to be cut into suitable sample pieces, which was performed in a -20 °C cold room.

An important part of this work was to date the ice core based on the information obtained from the analyses. To achieve this, knowledge of the Ice Core Dating software was necessary. Data from B01 was also available to help with the dating of the Belukha ice core 2018 (*B18*). This data could be used since there should be an overlap between the two ice cores. Black carbon concentration for the B01 was not measured, so data from another nearby glacier, Tsambagarav, was used instead.

The information obtained from the Belukha ice core will be used to determine recent changes in temperature and pollution in the Siberian Altai. The overall aim is to understand the climate response due to both natural and anthropogenic factors, to understand the climate dynamics in the past and try to predict future changes in the climate. The ice core record from 2001 will also be updated.

4 METHODS

4.1 Ion Chromatography

Ion Chromatography (IC) can be used to separate dissolved ions, i.e. cations and anions in a liquid solution. The IC (Metrohm 850 Professional IC) was used combined with an 872 Extension Module and an autosampler (858 Professional Sample Processor). This analytical technique consists of a liquid phase (the eluent) and a solid stationary phase. The stationary phase is inside of a column through which an eluent is continuously passed, with the help of a pump. The sample is injected and will travel together with the eluent to the column. The ions travel through the column with velocity, which depends on the ion affinity to the stationary phase. A conductivity detector is placed at the end of the column, and the concentration of the ions is plotted against the time in a graph that is called a chromatogram (Fig. 6.). The eluent used for the cations were 2.8 mM HNO_3. The most efficient way to separate the anions, was first to use an eluent with a lower concentration (1.5 mM Na_2CO_3/ 0.3 mM $NaHCO_3$) followed by an eluent with a higher concentration (8 mM Na_2CO_3/ 1.7 mM $NaHCO_3$). An autosampler was used to inject the samples automatically (Haddad, et al., 1990). The needle in the autosampler was washed with ultrapure water before every sample analysis. Ultrapure water is defined by > 18 MΩ cm resistance. One measurement for cations and anions was done for each sample.

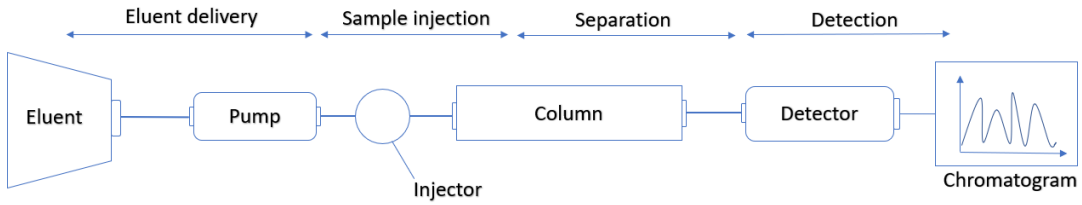

Fig. 6. Schematic image of the IC principle. It shows the eluent delivery, the sample injection, the separation in the column and the detection that produces the chromatogram.

4.2 Wavelength-Scanned Cavity Ring-Down Infrared Spectroscopy

Wavelength-Scanned Cavity Ring-Down Infrared Spectroscopy (*WS-CRDS*) is a highly sensitive laser-based absorption spectroscopy method. A laser diode enters the cavity, where a minimum of two highly reflective mirrors are located. The instrument used for this experiment was the Picarro L2140-i water analyzer (Picarro Inc., Santa Clara, Ca, USA) for isotopes and WS-CRDS will hereafter be referred to as Picarro. Picarro uses three highly reflective mirrors in the cavity, to enable the light wave to travel a longer distance. The laser

is turned on so that the cavity can be filled with the laser light. When the laser is turned off, the light inside the cavity will continue to bounce between the reflective mirrors. The light intensity will decrease to zero since the mirrors do not reflect 100% of the light. This decay is called the "ring-down" and it is measured by a photodetector. The Picarro has a cavity of 25 cm, which enables the laser light to travel over 20 km. The ring-down time is measured and only based on the reflectivity of the mirrors if the cavity is empty. The sample is vaporized and inserted into the cavity. The gaseous samples will absorb some of the laser light, which will accelerate the ring-down. The ring-down time for the empty cavity is then compared to the ring-down time for the cavity with gaseous sample, this can be seen in Fig. 7. The time for the gaseous sample will be shorter due to absorption of the laser light by the sample. (Berden, et al., 2000; Picarro, 2021). The needle in the autosampler was washed with ultrapure water before every analysis. Six measurements were obtained from every sample, the first three were not used, to minimize the risk of contamination.

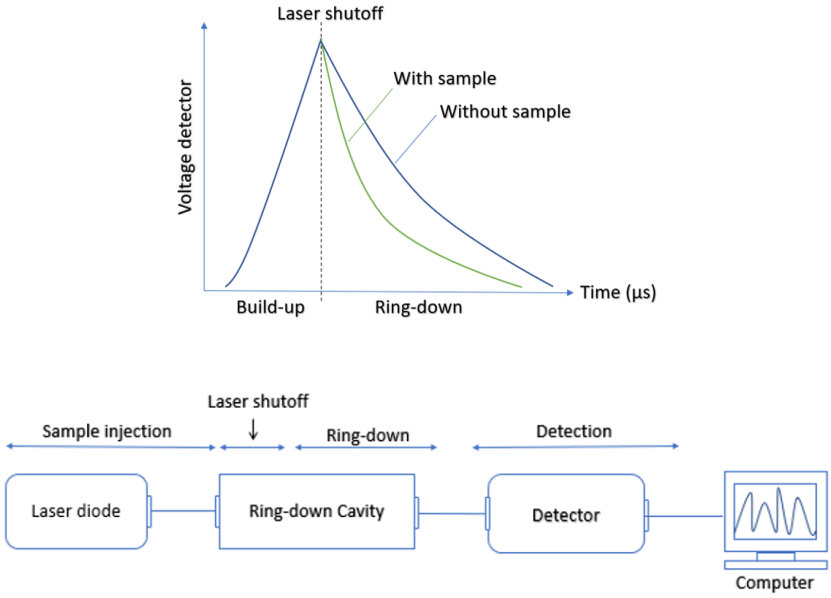

Fig. 7. Above is a diagram of the ring – down time with and without a sample, modified from (Berden, et al. 2000). Below is a schematic image of the Picarro, modified from (Picarro, 2021).

4.3 Single Particle Soot Photometer

Black carbon particle size and mass can be detected with the Single Particle Soot Photometer (*SP2*). The SP2 (Droplet Measurement Technology, Inc., Boulder, CO, USA) was used combined with an APEX-Q jet nebulizer system (High Sensitivity Sample Introduction System, Elemental Scientific Inc., Omaha, NE, USA). The sample is first nebulized and the droplets dried, the laser-induced incandescence of a particle determines the particles boiling point,

which can be used to determine the particle composition. The SP2 includes a diode-pumped neodymium-doped yttrium aluminum garnet laser and four detectors. Two of the detectors are optical detectors containing avalanche photodiodes (*APD*) and the other two detectors are incandescence detectors. The aerosols from the sample crosses the laser beam produced by the laser crystal in a perpendicular direction (Fig. 8.). The aerosols scatter light, which is detected by the APD. There are two filters that select specific wavelengths, i.e. 630 to 800 nm and 350 to 800 nm. A voltage signal is then produced from the APD, which is proportional to the scattering intensity. The light scatter is used to determine the size of BC particles. Particles with light absorbing material will be heated, absorbing the laser until they incandesce. The emitted light wavelengths will be proportional to the incandescence temperature, this light is collected by the incandescence detectors. The mass of the particle can be determined from the measured incandescence (Gao, et al., 2007; Baumgardner, et al., 2004).

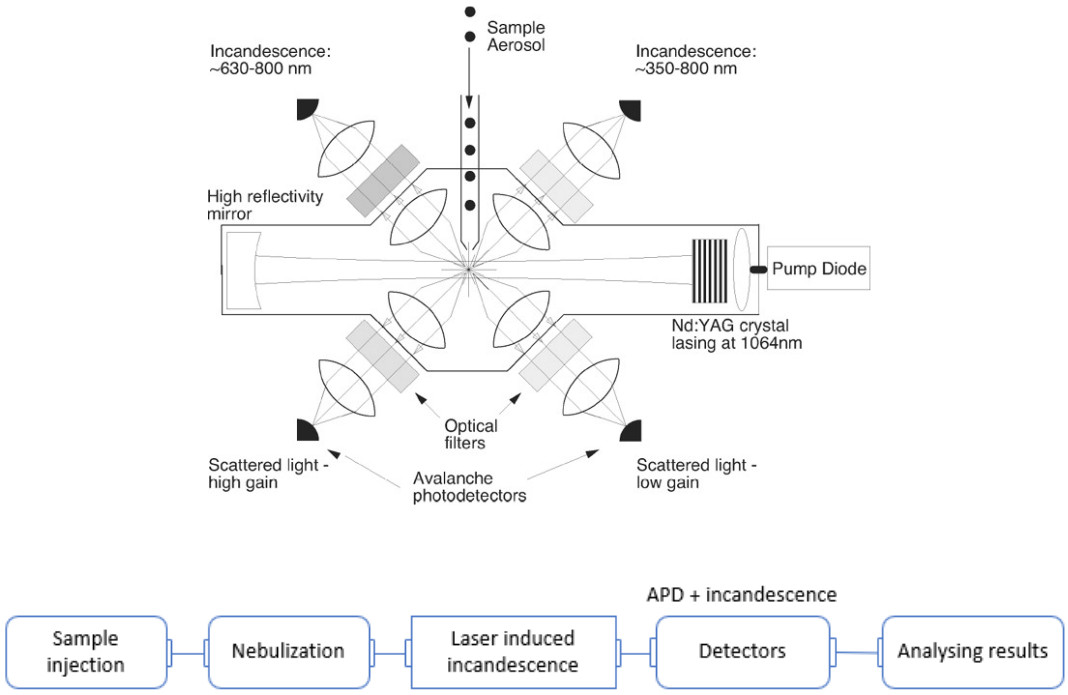

Fig. 8. Above is a schematic image on the SP2 detection (Gao, et al., 2007) and below is a schematic figure of the SP2 principle.

5 EXPERIMENTAL PART

For this laboratory work, cleanliness and preparation were of utmost importance to reduce the risk of contamination. The experimental parts were therefore conducted with "super-clean gloves". Different gloves were examined to see which ones were the cleanest to work with, i.e. the gloves that released the lowest amount of ions (analyzed with IC). It turned out that the polyethylene gloves from Coop, which is a retail and wholesale company in Switzerland, were the cleanest. A considerable amount of preparation was needed before the actual ice core cutting and analysis could begin.

5.1 Preparations and ice cutting

New 50 ml polypropylene vials with lids were used for the analysis of major ions, BC and trace elements and polyethylenterephthalate (*PET*) jars with lids were used for the organic carbon (*OC*) measurements. The term OC will from now on refer to both particulate organic carbon (*POC*) and dissolved organic carbon (*DOC*). The vials and jars were washed with ultrapure water since ultrapure water is purified and to a high degree deionized water. Containers with the vials and lids were filled with ultrapure water and, thereafter, shaken carefully to remove any additional air. Ultrapure water was then added again until the containers were completely full. The vials and lids were soaked in the ultrapure water for 24 h, before the ultrapure water was refilled. This process was repeated five times for all containers. Thereafter, the vials and the lids were dried in an oven for 24 h at 60 °C. The vials were labelled with a printed sticker containing all the necessary information. Different colors were used for the vial racks to minimize the risk of mix-up between the different samples.

Cutting schemes were calculated and designed depending on the analysis method and the density of the ice core. Five ice cores could usually be cut with the same cutting scheme, after which the increase in density had to be considered. The aim when calculating and designing a cutting scheme was to obtain enough ice for the analysis without wasting any of the ice core, since it is expensive to obtain. The minimum volume of sample needed for the OC analysis corresponds to about 250 ml. The OC samples had to be cleaned with ultrapure water before the measurements; therefore, the largest pieces of ice were selected to minimize ice loss. The volume of ice needed for the IC and BC analysis had to correspond to 6 ml melted sample. Otherwise, the concentrations would be too small to determine (see Equation 3.-4. and Fig. 9). The higher the density was, the less ice volume was needed to

achieve the minimum mass and volume of melted sample required. The sample resolution for IC and BC samples was usually around 8 cm.

$$OC, BC\ and\ major\ ions\ volume\ (ml) = \frac{Resolution\ (cm) x\ Area\ (cm^2) x\ Density\ (g/cm^3)}{100}$$

Equation 3. Calculations for the required sample volume, for the analyses of OC, major ions and BC. The water density used in these calculations are 1.0 g/cm³.

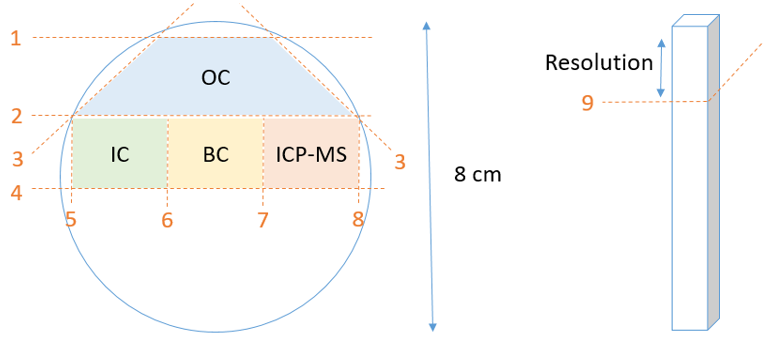

Fig. 9. A general cutting scheme for the ice cores. The left side shows a diagonal cut through the ice core. The orange numbers highlight the order of the cuts. The right side shows the resolution cut (i.e. the length of the sample). See also Fig. 11.

The ice cores were cut in a cold room at a temperature of -20°C. It is of utmost importance that the cold room is clean. The light table was cleaned three times with ethanol. Regular paper towel was used the first two times and a special polyester tissue, designed for use in super-clean rooms was used the third time. The plexiglas saw table and the stainless-steel band saw blades were thoroughly cleaned with acetone three times, always using the special polyester tissue. This cleaning process was performed before and after each cutting session. The instruments were also cleaned in-between every ice core. The reason for using pure ethanol and pure acetone is because of their good miscibility with water and organic compounds. They can be used in the cold room since their freezing points are -114.1 °C and -95 °C, respectively. Blank ice was used to check that the cutting scheme was functional and that the cold room and instruments were clean. To produce the blank ice, plastic containers were washed and filled with ultrapure water. The containers had to be stored in the cold room for two days to become fully frozen. The blank ice was cut at multiple stages of the process; it was first cut before the ice cores, then after the ice cores were cut and, lastly, after the saw table was cleaned. The length, diameter and mass of the ice core were measured and noted on a core sheet. Photographs were taken, two with the ceiling light on and two with the ceiling light off to better visualize the ice lenses (see Fig. 10.)

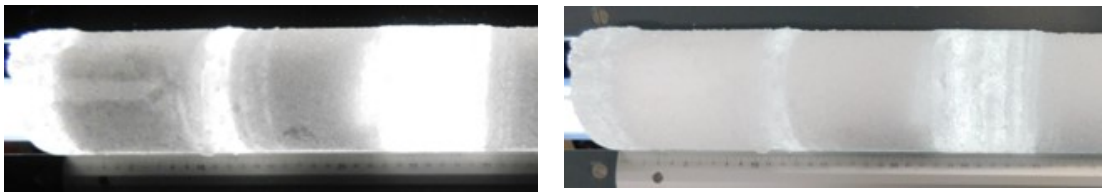

Fig. 10. Two photographs of ice core number 182 on the light table. The photograph to the left is photographed with the ceiling light turned on and the photograph to the right is photographed with the ceiling light turned off. Photographs taken by Petr Nalivaika.

The outer part of the ice core was removed to avoid any possible contamination from the drilling and the handling of the ice core. This outer part was approximately 0.2 cm thick. Broken edges were also decontaminated in the same way. The upperpart of the ice core was first cut, to keep the chronological order intact. The risk of mix-up could be reduced by always cutting and placing the pieces in the same way. The ice cores at the top consisted of mostly of firn, which made them more breakable. The cut ice samples were placed in respective vial or jar and stored in the cold room until measurements were carried out. The rest of the ice core was placed inside the ice core tube again and stored in the cardboard boxes for future analyses.

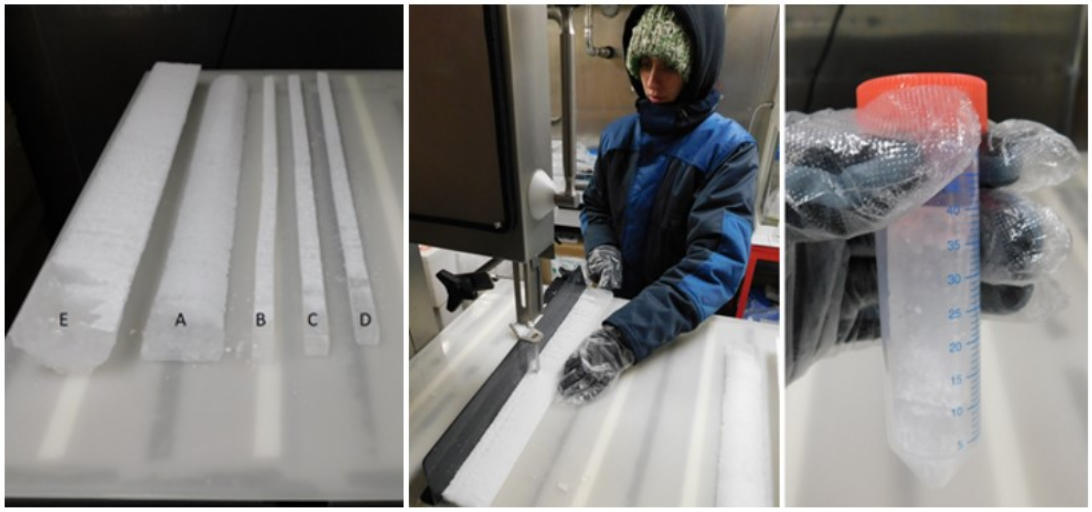

Fig. 11. To the left is the saw table and the cut ice core. Part A (OC sample) was first cut of, thereafter were part B (IC sample), part B (BC sample) and part C (ICP-MS sample) cut. Part E is the rest of the ice core that was stored for future analysis. The middle photograph illustrates the process of ice cutting. The right photograph illustrates the final product from the cold room. Photographs taken by Petr Nalivaika.

5.2 Analysis of major ions

The first 39 ice cores were cut, which resulted in 334 samples for the IC, SWI and BC analyses. This work will not focus on the OC or ICP-MS part anymore because of the time limit for this master's thesis. N_2 gas was blown for 20 s on the frozen IC samples, to reduce the risk of contamination of the sample with laboratory air. The N_2 gas creates a protective layer on the sample, since it replaces the laboratory air. Around 48 samples were melted (at room temperature) at a time, which is approximately the number that can be analyzed in 24 h. Before the IC samples were analyzed, 1 ml of the IC samples was pipetted into a 2 ml labelled vial for the SWI analyses. A new pipette tip was cleaned three times with ultrapure water before the sample was pipetted. The lids were unscrewed from the IC vials and a layer of aluminum foil was placed on the top. Thereafter, the vials were placed in the IC autosampler and measured. The analyzed cations were sodium (Na^+), ammonium (NH_4^+), potassium (K^+), magnesium (Mg^{2+}) and calcium (Ca^{2+}). The anions analyzed were fluoride (F^-), acetate (OAc^-), formate ($HCOO^-$), methanesulfonic acid (*MSA*), chloride (Cl^-), nitrate (NO_3^-), sulphate (SO_4^{2-}) and oxalate ($C_2O_4^{2-}$). Ultrapure water was used to wash the sampler needle in-between every sample. A snow sample from Jungfraujoch with known ion concentrations was measured randomly in-between samples. The sample from Jungfraujoch functioned as a control sample, to check that the values were correct. Before the samples were removed from the auto-sampler, the concentration for every ion was checked. Their detection limits (*LOD*) are given in Table 1. If the measured ion value was higher than the maximum value for the standards, the sample had to be re-measured. The sample was then diluted by a factor of two, which means that their concentrations were lowered by 50%.

Table 1. The limit of detection (LOD) for the analyzed species.

Ion	LOD (ppb)
Sodium	1
Ammonium	1
Potassium	2
Magnesium	5
Calcium	5
Fluoride	0.5
Acetate	2
Formate	0.5
MSA	0.2
Chloride	3
Nitrate	3
Sulphate	10
Oxalate	3

Some IC samples had to be re-measured due to too high concentration values. This only happened for formate and sulphate (see Appendix A). The data received from the IC analysis was calibrated with the standards and integrated manually for every sample. The mean value for the ions in the ultrapure water (i.e. the ionic background) was calculated and then subtracted from respective ion-sample value to obtain the correct value for the samples.

5.3 SWI data analysis

Three different standards were used for the SWI analysis. One was ultrapure water from the lab and the others were melted snow samples from Rueras and Scuol, respectively. Snow samples from these two mountains in Switzerland have been analyzed multiple times at PSI and have a known stable isotope composition. These SWI standards cover the range of $\delta^{18}O$ from -10 to -25 ‰, which is within the range for the Belukha ice core samples. Ultrapure water was used to wash the needle in-between every sample. The sample amount needed for one measurement was 10 µL melted ice. One sample was in total measured six times, the first three measurements were discarded to avoid contamination from previous samples, i.e. the memory effect. In the end, the mean value from the last three samples were used, unless some of the values deviated too much, in that case, an exception could be made and one of the first three measured values could be used instead. These exceptions had to be made if the standard deviation for $\delta^{18}O$ exceeded 0.1‰ or if the standard deviation for δH exceeded 0.5‰. The standard deviation values were obtained from the uncertainty of measurements from the IAEA certified standard. The need to re-measure a sample arouse if the mean value of H_2O was less than 17000 ppm or more than 23000 ppm. Not enough sample was injected if the value was below 17000 ppm and too much sample was injected if the value was above 23000 ppm. Both the $\delta^{18}O$ and the δD values are depending on the injected H_2O content. The re-measured samples can be seen in Table 2.

Table 2. The mean H_2O values and limits obtained from the stable water isotope measurements. The measured values and re-measured values are shown as the average values from the six measurements that were conducted for each sample.

Sample	Limits for mean H_2O value	Measured value	Re-measured value
91	17000 - 23000	17924.33	19616.00
92	17000 - 23000	11109.00	20028.33
93	17000 - 23000	14175.50	19952.33
94	17000 - 23000	16929.17	19572.67
244	17000 - 23000	22443,17	19302,67
245	17000 - 23000	24170,17	18678,67
246	17000 - 23000	25032,17	19523,33
287	17000 - 23000	19655,50	19195,00
288	17000 - 23000	19626,17	19193,33

Sample 91 and 244 were technically inside the range, but it was decided to remeasure the samples, since the values for the two following (i.e., sample 92 and 245) samples were outside the limits for the mean H_2O value. Samples 287 and 288 were remeasured due to human error in the lab. The values for the samples were calibrated from the standards, and drift corrections were made for both the $\delta^{18}O$ and the δD values. The drift corrected values for the standards were used due to showing more exact values. The deuterium excess was also calculated by using Equation 2 in section 2.1.

5.4 BC analysis

The black carbon samples were melted in room temperature sonication bath. The duration of the sonication was noted. The BC instrument measured particles until the limit of 1000 particles was reached. The number of BC particles will decrease by 4% to 16% in 6h when the sample has melted, it is therefore difficult to obtain a correct value through a remeasurement (Osmont, et al., 2018). The system was automatically cleaned before the measurements began. All standards were measured before the BC sample measurements began. One randomly picked standard was measured in-between a set of 20 BC samples. The needle was cleaned with ultrapure water between every measurement. Flow controls were done occasionally to check that everything was working correctly (see Equation 4.). A suitable flow rate was ~0.3 ml/min. Certain BC samples were remeasured due to low values, which could indicate a problem with the flow rate. Although, it could just be a sample with a naturally smaller number of particles. (Table 3.).

$$\boldsymbol{Flow\ rate}\left(\frac{\boldsymbol{mL}}{\boldsymbol{min}}\right) = \frac{\boldsymbol{Initial\ mass\ (g) - Final\ mass\ (g)}}{\boldsymbol{Measurement\ time\ (min)}}$$

Equation 4. Calculation of the flow rate for black carbon measurements. The density of the sample is assumed to be 1g/ml.

Table 3. The BC measured and re-measured values.

Sample	Measured value (ppb)	Re-measured value (ppb)
1	0.070	8.905
2	0.071	7.096
3	0.309	4.019
4	3.334	3.114
32	9.582	9.509
33	0.071	3.471
91	1.833	1.768
92	0.964	0.880
93	0.306	1.219
113	0.342	0.285
126	0.444	0.367
127	0.917	0.990
181	39.146	52.819

Standardized values were used as a reference point in the calibration of the sample values. The ultrapure water values were divided from the measured sample values. These values were plotted against the concentration of the standards in a diagram to obtain a calibration curve and an equation for the linear line by use of least square analysis (in Excel). The equation from the first measurements were used, since the number of particles will decrease with time. The BC signal was measured with an incandescence detector, where the output signal is named BHNL. The equation y=0.1292x+0.0189 for the calibration curve was obtained. This calibration curve shows how the incandescence signal is transferred into BC concentration, based on the standards. In the equation, y is the BC concentration in ppb and x is the incandescence signal (BHNL).

6 RESULTS AND DISCUSSION

6.1 Contamination

To understand how important cleanliness is in this work, the first analyzed IC sample was a "finger-test". When a finger is dipped in ultrapure water for a couple of seconds, ions transferred from the skin to the solution. The most elevated values for the "finger-test" compared to the ultrapure water are highlighted in Table 4 with a light blue color. The reason for elevated values of sodium, chloride, potassium, and acetate can be explained by sweat from the skin. The high value of acetate originates, however, most likely from nail polish and calcium from the nails. The elevated value for nitrate is uncertain.

Table 4. Ion concentration of the "finger-test" compared with the mean value of ultrapure water.

Ion	"Finger-test" (ppb)	Mean value of ultrapure water (ppb)
Sodium	69.75	< LOD
Ammonium	0.83	< LOD
Potassium	157.58	< LOD
Magnesium	3.30	2.14
Calcium	12.37	2.81
Fluoride	0.00	< LOD
Acetate	640.74	1.64
Formate	2.55	1.77
MSA	0.00	< LOD
Chloride	129.15	3.14
Nitrate	15.38	4.73
Sulphate	9.93	5.79
Oxalate	1.89	0.95

The results from the blank ice were compared to the "finger-test" and were considered not to be contaminated. Blank ice was cut during three different stages of the entire cutting process: before the ice cores were cut, after the ice cores were cut and after the saw table was cleaned. Three ice samples of blank ice were obtained from each of these stages. They were analyzed with IC and the mean value for each stage was calculated (see Table 5.). The values before cutting and after cleaning are in good agreement. The values after cutting are slightly elevated compared to the two other columns. This means that there is some minor contamination between the ice cores; the values are, however, quite low. It is quite difficult to avoid all cross contamination between different ice cores. However, these values remain satisfactory.

Table 5. The ion concentration of blank ice for the three different ice cutting stages.

Ion	Before cutting (ppb)	After cutting (ppb)	After cleaning (ppb)
Sodium	< LOD	1.21	< LOD
Ammonium	< LOD	< LOD	< LOD
Potassium	< LOD	0.42	< LOD
Magnesium	2.23	2.66	2.93
Calcium	4.17	10.31	4.37
Fluoride	0.00	< LOD	< LOD
Acetate	10.56	13.29	15.86
Formate	4.77	6.71	7.24
MSA	< LOD	< LOD	< LOD
Chloride	< LOD	2.46	< LOD
Nitrate	3.62	6.17	4.11
Sulphate	5.39	7.45	5.34
Oxalate	1.52	1.81	1.49

6.2 Ice core dating

Every ice core is different, and the dating methods vary much. One usually starts by pinpointing a reference horizon. The first expected reference horizon in the B18 ice core would be the tritium peak from the nuclear testing in 1963 (Eichler, et al., 2000). However, we did not estimate that this part of the ice core would extend so far back in time. The depth was converted from cm to meters of water equivalent (m w.eq.) (see Equation 5.) to account for varying density. For this work annual layer counting was used, plus a reference horizon from B01, see below.

$$\boldsymbol{Depth\ (m\ w.eq.)} = \frac{\boldsymbol{Depth\ (cm)\ x\ Density\ (g/cm^3)}}{\boldsymbol{100}}$$

Equation 5. Converting depth in cm to depth in m w.eq.

6.2.1 Determination of the year 2001 in B18

The depth of the analyzed part of the ice core was known (17.1 m w.eq.), and the next step was to determine which year this depth would correspond to. The average annual snow accumulation rate for the B01 was used to roughly estimate the age, and the rate was 0.56 m w.eq. (Eichler, et al., 2009a). There are 17 years between the drilling of the two ice cores from the Belukha. If one were to multiply 17 by 0.56 m w.eq., one would obtain the rough estimation that the year 2001 in the B18 would be at a depth of 9.52 m w.eq.. This represents a roughly estimated value only since the average snow accumulation varies from year to year.

The data for ions and stable water isotopes from B01 and B18 was compared to determine the year 2001 more exactly. By plotting the data from B01 with the data from B18 and further wiggling the data until a match was found, a good overlap could be found. The data from B01 shows a peak in the calcium concentration at year 2000-2001 (Fig. 12.). This calcium peak was used when the two data sets were compared. The most intense calcium peak (at 10.6 m w.eq.) match extremely well when the depth for B01 was changed from 9.52 m. w.eq. to 10.1 m w.eq.. The values for both B01 and B18 are calculated as 3-point moving averages to make it visually easier to match. The ion concentration was expressed in µeq/L instead of ppb. (Equation 6.) The match was checked for other ions as well as for SWI.

$$\boldsymbol{Concentration\ (\mu eq/L)} = \frac{\boldsymbol{Ion\ charge}}{\boldsymbol{Molar\ mass\ (g/mol)}}\ \boldsymbol{x\ Concentration\ (ppb)}$$

Equation 6. Converting ion concentration from ppb to µeq/L.

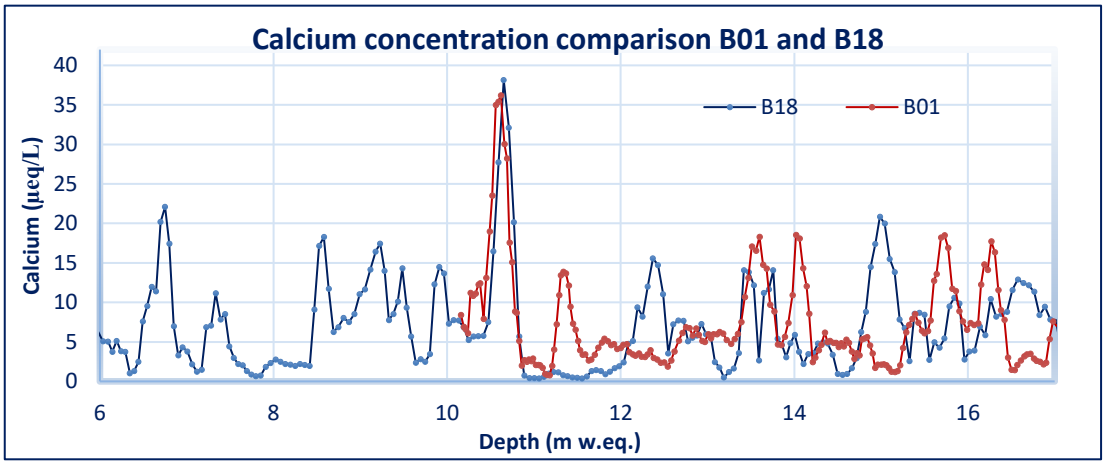

Fig. 12. Calcium concentration comparison of B01 and B18 at a depth of 10.1 m w.eq.. The concentration is given with a 3-point moving averages to make the lines smoother.

6.2.2 Determine the last year in B18

The match between B01 and B18 is convincing in the beginning (see Fig. 12.). Further down agreement is less good, likely due to variability in the snow accumulation. The depth of 10.1 m w.eq. would, therefore, not be true for the end of this ice core part. The last year was estimated on the depth of year 2001. The estimation can also be based on the depth for year 2018. The time difference will be longer for 2018 compared to 2001 to the last year and, therefore, more uncertain (Equation 7.).

$$\mathbf{2018}: \frac{\mathbf{17.1\ m\ w.eq.}}{\mathbf{0.56\ m\ w.eq./yr}} = \mathbf{30.5\ yr} \rightarrow \mathbf{1987.5}$$

$$\mathbf{2001}: \frac{\mathbf{10.1\ m\ w.eq.}}{\mathbf{0.56\ m\ w.eq/yr}} = \mathbf{18\ yr} \rightarrow \mathbf{1983}$$

Equation 7. Estimated calculations for the last year based on the depth of year 2018 and 2001.

By wiggling the two data sets, it was detected that the end matches at a depth of 8.9 m w.eq. of B01. The ammonium and sulphate matches are very clear, and the sulfate peak is very distinctive (see Fig. 13). The $\delta^{18}O$ data sets do not agree well with each other, which is most likely due to meltwater percolation. Since the B01 is dated, it is easy to check which year this peak would correspond to. The end of the ice core corresponds to the year 1985. This also proves that the estimation made from the depth of year 2001 is more accurate than the estimation made from the depth of year 2018.

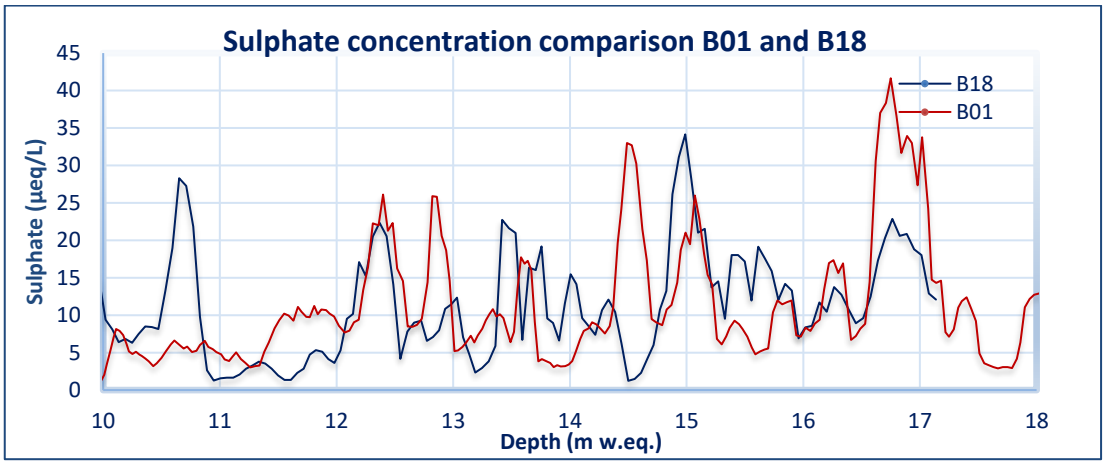

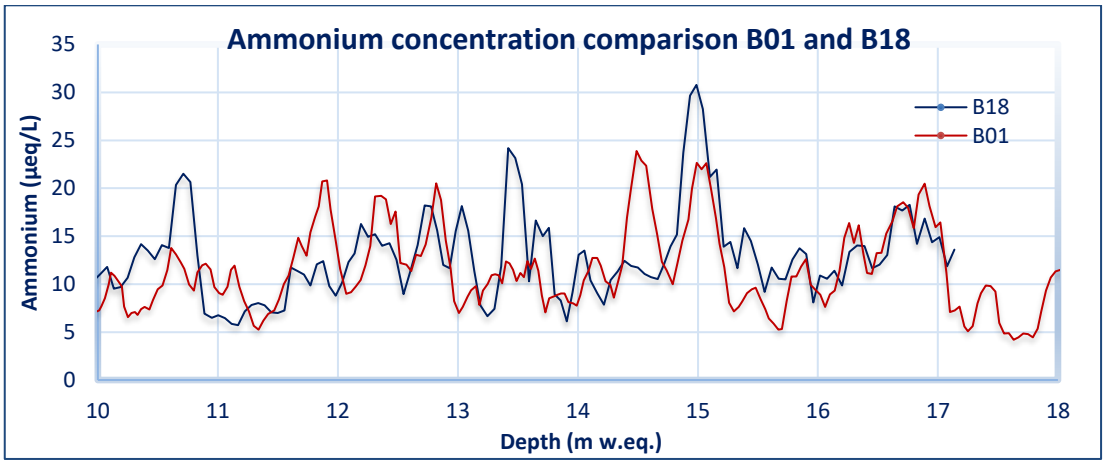

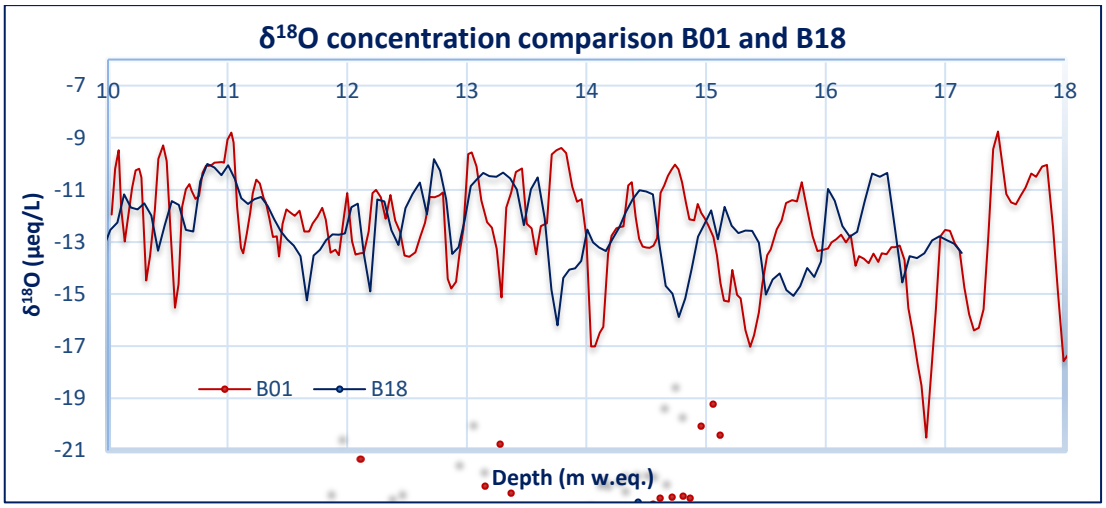

Fig. 13. Sulphate, ammonium and $\delta^{18}O$ concentration comparison of B01 and B12. The concentration is given with a 3-point moving averages to make the lines smoother.

6.2.3 Determination of years based on annual signals

The seasonal signals from ions and SWI were used to attribute years in the ice core. This was done with the Ice Core Dating software. This program uses ice core glaciochemical records to create a depth-age scale. One can choose which signals to use in the program. Here, the signals used are 3-point moving averages, to visualize the shown trends more easily. An attempt was made to date the ice core with the original values, which turned out to be difficult because all the details made it complicated to visualize the entirety. This software cannot process negative values, which was a problem for the negative values for SWI. To solve this problem, the number 25 was added to all $\delta^{18}O$ values. The $\delta^{18}O$ values (see Fig. 14.) should be within the range of (-25) – (-10) instead of 0 – 15. The three known years were first pinpointed in the software, before the annual layers were chosen. The first known year was 2018 when the ice core was drilled, and the years 2001 and 1985 were determined from matching in Excel. Since the ice core was drilled during the summer, the year 2018 could not be placed at the beginning of the diagram, since it is year 2018.5.

When the three pre-determined years (2018, 2001 and 1985) were placed, the years with clear winter minimum were added. For the annual layer counting, much focus was put on ammonium, calcium, sulphate and the stable water isotopes. These ions exhibit good seasonal variations in deposition on the glacier. The maximum deposition of these chemical species will occur during summer, which means that the minimum concentration between two peaks would be the beginning of a new year. The minimum values for $\delta^{18}O$ corresponds to the winter and, therefore, also to the beginning of a new year. When these lines were

determined, it was important to check the accumulation rate between the years. The software program automatically calculated the accumulation for each year, and in this way, one could see if the potentially added years were much too long or much too short. It is quite unlikely that one year would have the accumulation rate of 1 m w.eq. or only 0.1 m w.eq.

A screenshot of the work done in the Ice Core Dating software was taken (see Fig. 14.). The calcium peak that was used to determine the year 2001 in B18 can clearly be seen as well in the screenshot. The three pre-determined years are shown with yellow lines and the placed years are shown as dark blue lines. The period from 1995 to 2000 was more difficult to date, due to loss of annual signals; this area is marked with a light rectangle. The red arrows show some contradiction with the dating, which will be discussed in the next chapters.

Taking a closer look at the different years in Fig. 14, one can tell that the years 2015, 2000, 1998, 1995, 1990 and 1987 are placed on the $\delta^{18}O$ maximum. This contradicts the idea of placing a year at the minimum of the $\delta^{18}O$ signal. Since the shown signal was with a 3-point moving average, it was decided to take a closer look at the $\delta^{18}O$ at the problematic areas, without the 3-point moving averages.

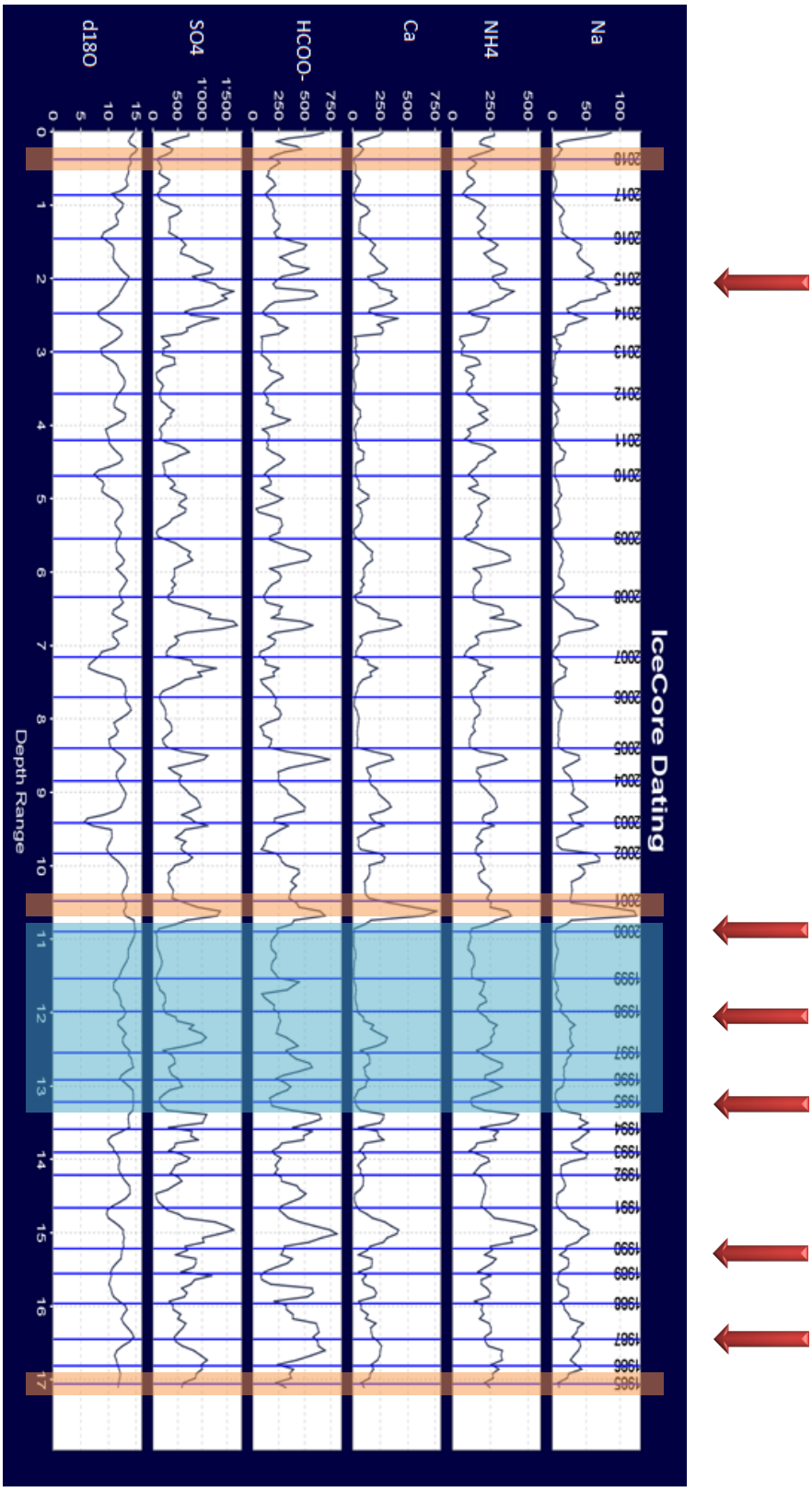

Fig. 14. Screenshot from the Ice Core Dating software. The orange lines show the three known years. The red arrows show the contradictory of placing a year at maximum of the $\delta^{18}O$ peak. The blue area shows the most difficult part to date, due to weak seasonal signals.

The $\delta^{18}O$ signal was plotted against the depth without the 3-point moving averages, which can be seen in Fig. 15. Without the 3-point moving average, there is a small minimum for $\delta^{18}O$ at the depth of 194.5 cm w.eq.. This minimum could not be seen due to the smoothened 3-point moving average lines. The orange line (see Fig. 15.) shows where the year 2015 was pinpointed. The graph also shows the amount of ice lenses at that depth. Ice lenses must be considered when it comes to the accuracy of paleoclimatic reconstruction. Ice lenses are formed due to melting, percolation and re-freezing of water. Meltwater percolation can elute chemical species and affect isotopic enrichment, which decreases the seasonal signals. To confirm the hypothesis that meltwater percolation would have shifted the $\delta^{18}O$ signal, the photograph of ice core 174 (depth of 200 cm w.eq.) was checked. Meltwater percolation can clearly be seen in the photograph as light vertical lines (see Fig. 15.).

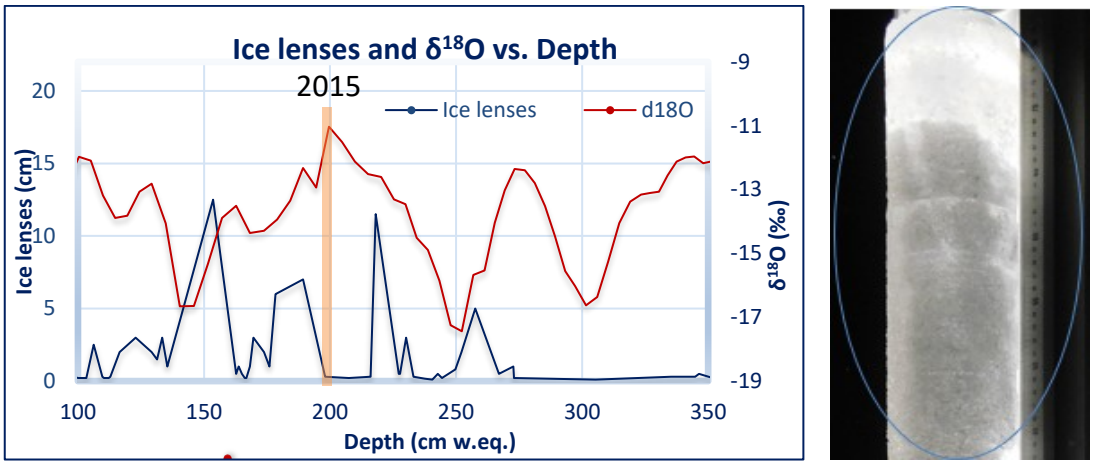

Fig. 15. To the left the $\delta^{18}O$ value and the amount of ice lenses are compared to the depth corresponding to year 2015. The year 2015 is marked with an orange line. To the right a photograph of ice core 174. Meltwater percolation can be seen at the end (i.e. at the top) of the ice core.

The other years were also checked. Fig. 16 shows where the years 2000, 1998, 1995, 1990 and 1987 were pinpointed. The years are pinpointed at the maximum, the minimum is just very small. The seasonal signal for $\delta^{18}O$ is decreased and shifted, due to meltwater percolation. With this confirmation, that the years were not actually placed at the $\delta^{18}O$ maximum, the dating was completed with the Ice Core Dating software.

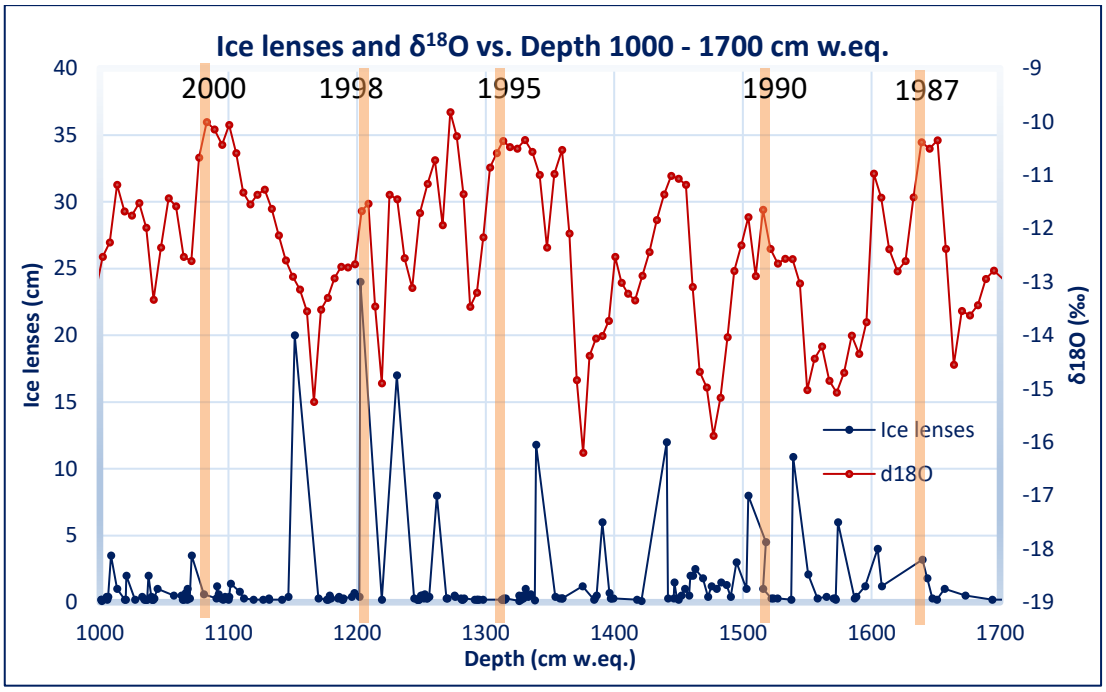

Fig. 16. $\delta^{18}O$ value and the amount of ice lenses compared to the depth corresponding to year 2000-1987. The years are marked with yellow lines.

The corresponding depth for every year and the annual accumulation obtained from the Ice Core Dating Software are presented in Appendix B. The average annual accumulation rate for this part of the B18 is 0.51 m w.eq.. The dating conclusion is that this part of the B18 extends back in time to the year 1984.7 at the depth of 17.10 m w.eq..

6.2.4 Corroboration of the ice core time scale

To finally prove that the dating is correct, the records of B18 were compared using the presented time scale. MSA, fluoride, acetate and BC were not analyzed for B01, and could therefore not be compared with B18. Average annual values for the other chemical species and SWI for the two ice cores were compared. The comparison between the analyzed ions for the two ice cores showed a good match (see Appendix C). The concentrations are given as annual values to make it easier to visualize the match. This comparison confirmed the dating of the B18. The average annual accumulation rate was remarkably similar for the two ice cores, 0.56 m w.eq. and 0.51 m w.eq. for B01 and B18 respectively. This explains the good match for chemical species between the two ice cores. Annual records of chemical species agree well between the B18 and B01 core, corroborating the established dating and allowing to update the B01 records to 2018. The uncertainty for dating always exists and for the analyzed part of B18 it is set at one year. The entire B18, from top to bottom, is dated around 20000 years (Fang, et al., 2021).

6.3 Observations within B18

6.3.1 Ice lenses

Ice lenses could be seen throughout the analyzed part of B18. Most of the ice lenses were under 3 cm thick (Fig. 17.). Ice lenses show the amount of melting and re-freezing that has occurred on the glacier. Melting of summer snow on the surface, creates meltwater that percolates downwards. More melting occurred at 2-3.6 m, at 9.6-11.2 m, and at 19.5-25 m. It must be taken into consideration that percolation of meltwater can interfere with the annual chemical signals. The density of the ice core increases with depth until the maximum density is reached. The red dotted trendline in Fig. 17. clearly demonstrates this increase in density. The analyzed part of B18 (26.4 m) did not reach its maximum density; firn could be seen in all ice cores. The maximum density of ice cores is ~0.9 g/cm^3), which is the density of ice not containing bubbles. The minimum and maximum density of the analyzed part of B18 is 0.45 g/cm^3 and 0.81 g/cm^3 respectively (i.e., the orange line in Fig. 17.). The density is dependent on the amount of ice lenses, more ice lenses equal higher density, this can clearly be seen at the depth of 0-5 m (see Fig. 17.).

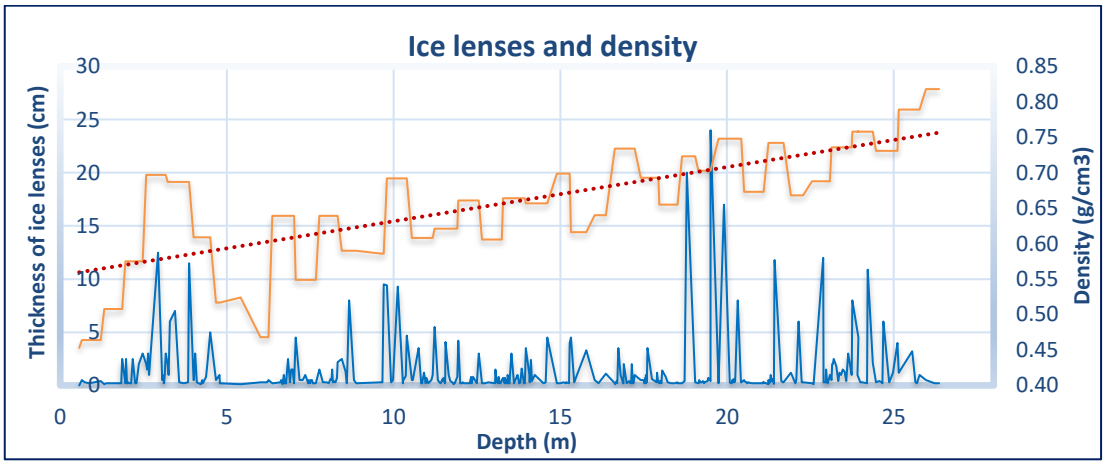

Fig. 17. The thickness of ice lenses (blue) and density (orange) versus total depth. The dotted red line shows the trendline for the density.

6.3.2 Airborne particles, visual dust layers, and insects

One dust layer was visually observed as a colored layer in the analyzed part of the B18. The observed dust layer was 1.5 cm thick at a depth of 7.59 m w.e.q., which represents the beginning of 2006. When a dust layer is observed, one can expect elevated concentrations of calcium and magnesium. An increase in concentration can be seen for both magnesium

and calcium (Fig. 18.). The increase in concentration is small due to the dilution of the dust layer. The dust layer was only 1.5 cm, and the resolution of the IC sample was 8.3 cm. The concentration increase would have been considerably higher if only the dust layer were sampled.

An insect was found in the IC sample 237, the insect is most likely a mosquito. As previously discussed, the wind can transport dust onto the glacier. Other debris, e.g. pollen and small insects can also be transported with the wind to the surface of the glacier. The insects are eventually covered by snow and finally entombed in the glacier when the transformation from snow to ice occurs. This insect was wholly preserved and found at a depth of 11.7 m w.eq., which corresponds to the summer of 1998. (see Fig. 18.).

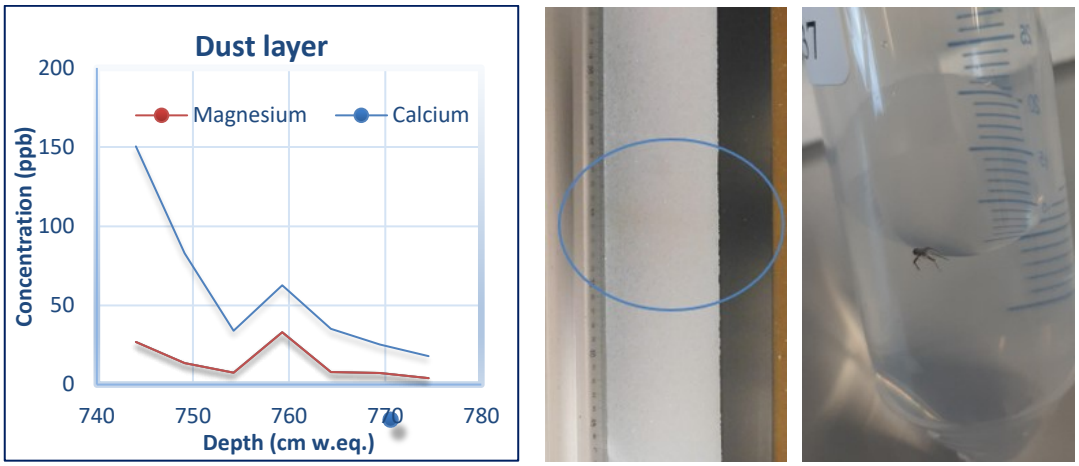

Fig. 18. The concentration of magnesium and calcium in ppb is shown against the depth in cm w.eq. in the left figure. The dust layer was seen in sample 164 at a depth of 759.3 cm w.eq., three samples before and after the sample with the dust layer is shown. The photograph in the middle shows the ice core 188 containing the dust layer (marked with a blue circle). To the right is a photograph of the insect found in IC sample 237. Photographs taken by Thomas Singer.

6.4 Major ion concentrations

An overall picture of the analyzed species can be seen in Table 6. The median values in the analyzed ice core varied between 1.2 ppb and 373.5 ppb. It can clearly be seen that the percent of anions sulphate, nitrate and formate are the highest. These anions clearly show the highest median value as well. The highest percent for cations are for ammonium and calcium. MSA and fluoride clearly show the lowest values. The concentration differences between the analyzed species are noticeably large. The concentration for fluoride (lowest) is 0.3% of the sulphate (highest) concentration. Appendix C shows a comparison between the ions analyzed in 2001 and 2018.

Table 6. The percent and median values for all analyzed species.

Ion (ppb)	Total concentration (ppb)	Median (ppb)	Percent (%)
Sulphate	175 112.2	373.5	32.6
Nitrate	109 170.6	275.5	20.3
Formate	95 020.1	224.5	17.7
Ammonium	68 388.1	183.2	12.7
Calcium	41 242.1	65.0	7.7
Chloride	10 122.7	19.6	1.9
Acetate	10 207.3	15.8	1.9
Oxalate	8 373.5	14.9	1.6
Sodium	6 814.8	12.0	1.3
Potassium	5 534.3	10.3	1.0
Magnesium	5 225.8	10.0	1.0
MSA	945.2	2.2	0.2
Fluorine	545.8	1.2	0.1

The correlation coefficient (r) between the analyzed ions can be calculated to investigate common sources for the different ions (see Table 7.). The strong correlation between almost all the chemical species is due to the seasonality of the concentration, which means that the correlation is due to similarities in the atmospheric transport and not in the strength of the emission source. To correct this, annual averages of the chemical species were used. The non-normal distribution was also corrected by calculating the correlation coefficient from $\log_{10}$[concentration]. The ions at the Belukha glacier mainly originates from dust (calcium, magnesium, sodium and chloride), anthropogenic sources (nitrate, sulphate and ammonium) and biogenic emissions (formate, oxalate and ammonium) (Henderson, et al., 2006).

One cannot expect a high correlation between $\delta^{18}O$ and the concentration of chemical impurities on a sample basis. The stable isotope values are smoothed by e.g. sublimation, diffusion, recondensation of water vapor in the snow, firn matrix triggered by temperature gradients. This does not affect the concentrations of chemical impurities, which do not sublimate.

Table 7. The ion correlation coefficients for 34 annual averages calculated from $\log_{10}$[concentration].

	Calcium	Magnesiu	Sodium	Chloride	Potassium	Formiate	Ammoniur	Nitrate	Sulfate	Acetate	MSA	Flouride	Oxalate
Calicum	-	0.91	0.79	0.49	0.71	0.44	0.61	0.73	0.87	0.15	0.28	0.23	0.86
Magnesium		-	0.82	0.45	0.69	0.45	0.67	0.67	0.85	0.21	0.28	0.21	0.86
Sodium			-	0.40	0.58	0.49	0.58	0.54	0.66	0.19	0.21	0.20	0.72
Chloride				-	0.30	0.37	0.39	0.50	0.41	0.00	0.05	0.25	0.51
Potassium					-	0.18	0.45	0.67	0.70	0.18	0.41	0.07	0.61
Formiate						-	0.65	0.28	0.23	0.13	0.00	0.42	0.52
Ammonium							-	0.69	0.57	0.23	0.13	0.25	0.68
Nitrate								-	0.75	0.13	0.40	0.11	0.65
Sulfate									-	0.10	0.45	0.10	0.76
Acetate										-	0.09	0.04	0.13
MSA											-	0.05	0.15
Flouride												-	0.28
Oxalate													-

6.4.1 Dust-related species

It can clearly be seen from the correlation coefficients in Table 7 that calcium, magnesium, sodium and chloride correlate well with each other. The believed source for these ions is mineral dust. The characteristic feature for dust-related species is the large maxima, which can clearly be seen in the summers of 1994, 2000, 2007 and 2014. (see Fig. 20.). These peaks are most likely due to increased dust particles from the arid region of central Asia. The main dust source areas are believed to be the deserts Kara-Kum, Kyzyl-Kum, Mojyn-Kum, Taklimakan and the Kazakh loess hills (Olivier, et al., 2006) (see Fig. 19.). Studies have shown that dust from the Taklimakan desert can be transported by the westerlies over long distances (5000 km) and reach elevations of up to 5000 m. This means that dust from the Taklimakan desert can reach the Altai Mountains (Sun, et al., 2001).

The main dust tracers are calcium and magnesium. A mineral group containing these minerals are the calcium-magnesium carbonates, e.g. calcite ($CaCO_3$) and dolomite ($CaMg(CO_3)_2$). Calcium and magnesium could also originate from anthropogenic sources, e.g. from cement production in areas close to the Altai Mountains. Deposition of mineral dust enriched with feldspars ($NaAlSi_3O_8$-$CaAl_2Si_2O_8$) can cause an increase in sodium and calcium. The large maxima for all the mineral dust ions show peaks at the same time, confirming the same origin. The dust origin is difficult to determine, since the main components in dust particles (i.e. Si, O and Al) were not analysed.

Fig. 19. Map of Asia showing the deserts as potential source areas for mineral dust in the Belukha ice core. The location of the deserts is shown as different shapes, Kara-Kum as a red circle, Kyzyl- Kum as an orange cross, Mojyn-Kum as a blue square and Taklimakan as a green triangle. Modified from (Henderson, et al., 2006).

Chloride and sodium both show a larger peak in the summer of 2001, which suggests an input of another mineral enriched in sodium and chloride. Halite (NaCl) is a common evaporite deposit mineral, so the increase in 2001 could be due to dust enriched with halite. The evaporite deposits originate most likely from the Aral Sea basin or from the Tibetan Plateau. Another explanation could be sea salt origin from a body of water. Examples of these water sources are the Atlantic Ocean, the Aral Sea, the Caspian Sea, the Mediterranean Sea and the Black sea. It can be argued that the contributions from oceans are negligible, due to the long distance from the ocean to the highly continental location. The chloride-to-sodium ration for Halite is 1.0 and for sea salt 1.16. The median value for chloride to sodium ratio for B18 is 1.05. It is difficult to distinguish these ratios, so the contribution from sea salt cannot be excluded. The increased chloride concentration can also originate from anthropogenic sources, e.g. hydrochloric acid from coal combustion (Olivier, et al., 2006). This would explain the good correlation between chloride and the anthropogenic species; ammonium, nitrate and sulphate (see Table 7.). Only one dust layer was observed in the analyzed part of B18, indicating that bigger dust storms reaching Belukha are rare phenomena.

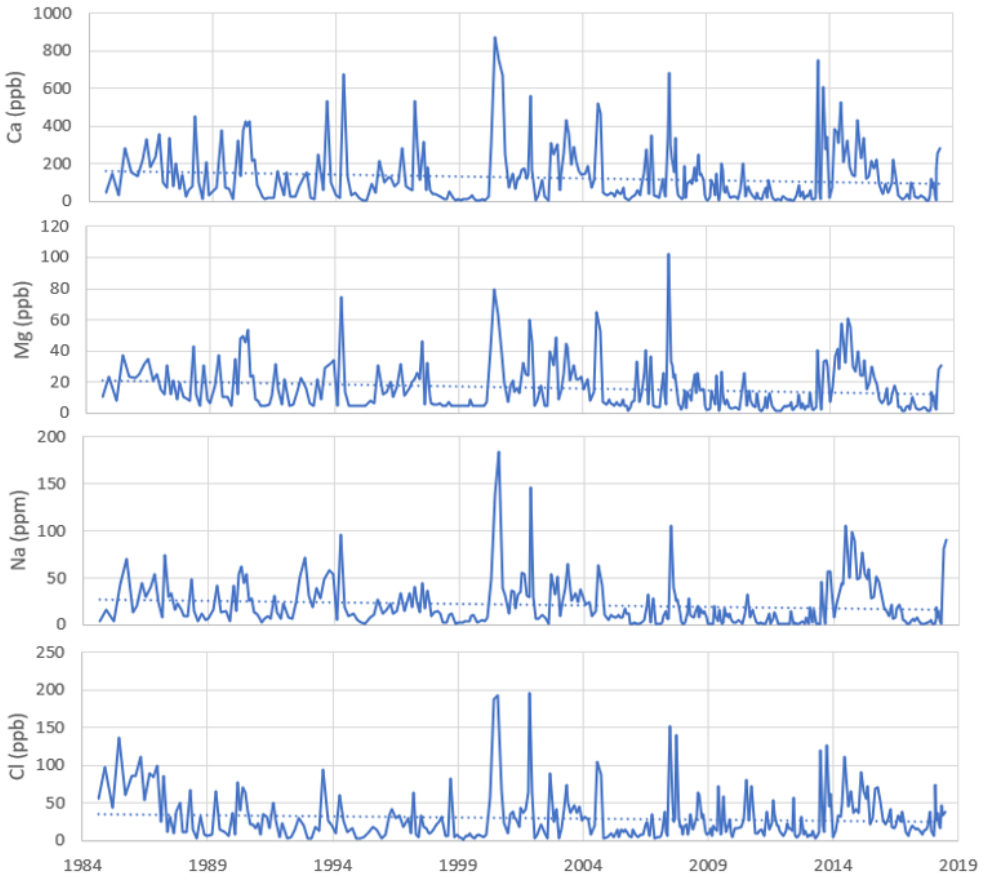

Fig. 20. Concentration in ppb for the dust-related chemical species, calcium, magnesium, sodium and chloride.

6.4.2 Anthropogenic-related species

A good correlation between nitrate, sulphate and ammonium can also be seen in Table 7, the source is believed to be anthropogenic. Ammonium correlates well with most of the ions, indicating several different sources. The anthropogenic species show good seasonal variation, and the match is clear. The largest peaks occur in 1990, 1994, 2000, 2004 2007, 2013 and 2014 (see Fig. 21). Ammonium emissions from livestock waste, fertilizer and bacterial decomposition would have common atmospheric transport like the other anthropogenic species (Olivier, et al., 2006). The correlation between ammonium and formate (r = 0.65) is very similar to the correlation between ammonium and sulphate (r = 0.57). This indicates that ammonium has various sources and cannot be attributed to only natural or anthropogenic origin.

The ions with the highest percentage in the analyzed part of B18 are sulphate and nitrate (see Table 6.), indicating a significant source. These two secondary aerosols originate from both anthropogenic and natural sources. The natural source for nitrate includes biomass burning, soil exhalation, lightning and cosmic rays. The anthropogenic sources include nitrate fertilizers, traffic emissions and all high temperature processes which oxidize atmospheric N_2 (i.e., industries and power plants) (Olivier, et al., 2006). The main part of sulphate emission originates from anthropogenic sources, namely SO_2 emissions from fossil-fuel burning. Several natural sources may influence the sulphate value, e.g. volcanic emissions, mineral dust and marine biogenic dimethyl sulfide (*DMS*) oxidation in oceans (Schwikowski, et al., 1999).

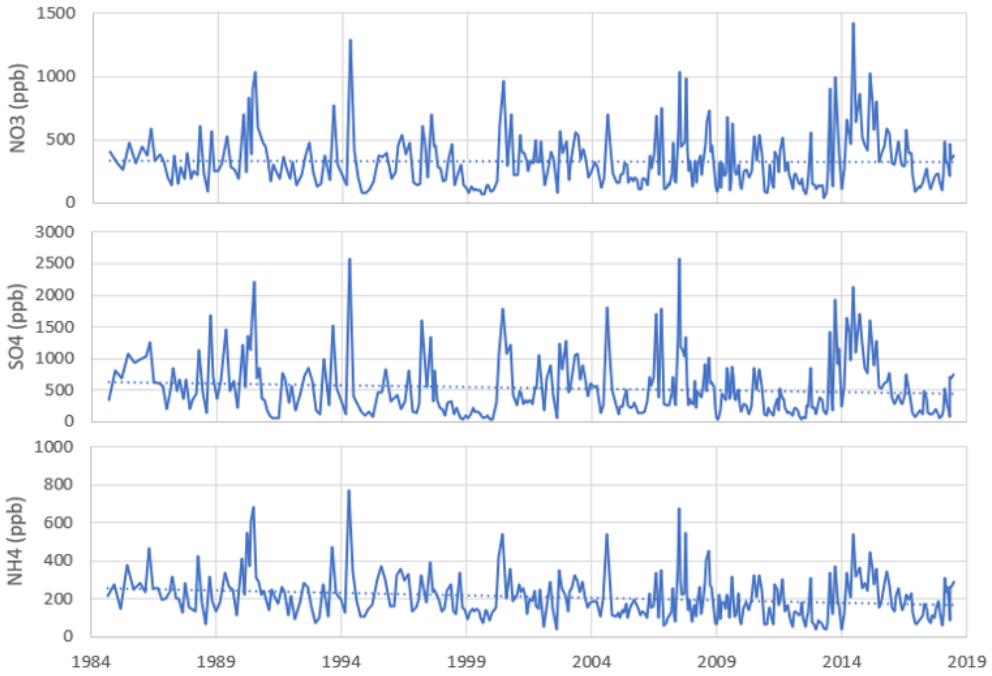

Fig. 21. Concentration in ppb for the anthropogenic-related species; nitrate, sulphate and ammonium vs. age.

6.4.3 Biogenic and biomass burning species

A strong correlation between formate, oxalate and ammonium can be seen in Table 7. The assumed source is biogenic and biomass burning emissions. Ammonium and carboxylic acids (that form oxalate and formate) are released from both biogenic and biomass burning emissions (Olivier, et al., 2006). Formate and ammonium have the third and fourth highest concentration in the analyzed part of B18 (see Table 6.). The source from where formate and ammonium originate needs to be considered, the most likely source being the biomass in Siberia. The concentration trend for formate differs slightly from the other biogenic emission species. There are two distinctive peaks for the three biogenic emission species, in 1994 and around 2014 (end of 2013 or beginning of 2014) (see Figure 22.). Two other peaks for formate can additionally be seen in 2003 and 2015 which, in turn, are not so distinctive for oxalate and ammonium. Beyond this, there are common peaks for oxalate and ammonium in 1990, 2000, 2004 and 2007 (see Figure 22.). The peak difference could be due to different biomass which was burnt or different conditions during the fire.

The strongest seasonal fluctuations can be seen for the biomass species (see Fig. 22.). This is most likely due to the annual growing season and seasonality of temperatures, which increases the vegetation. Fires are mostly ignited during the warmer season (Olivier, et al.,

2006). The ammonium peaks may differ, since ammonium correlates well with almost all the analyzed species, indicating several sources for ammonium (see Table 7.).

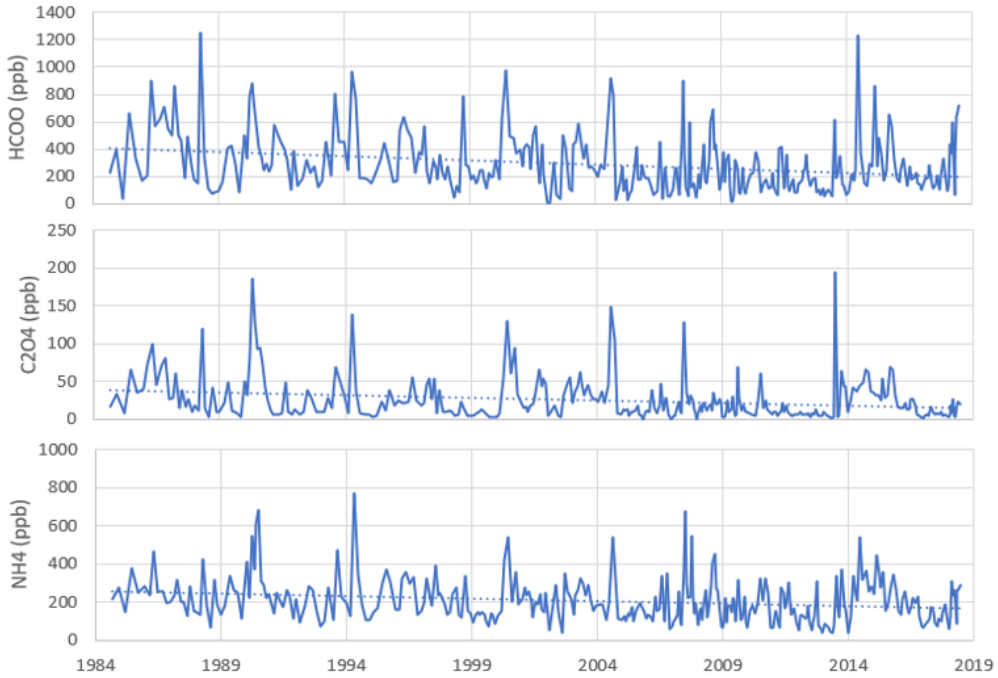

Fig. 22. Concentration in ppb for biogenic and biomass burning species; formate, oxalate and ammonium.

6.4.4 Other analyzed species

Potassium show high correlation with all species except for acetate, formate and fluoride (Table 7.). This indicates several different origins for potassium. The correlation to the dust-related species could be explained by evaporite deposits of potassium-rich feldspar ($KAlSi_3O_8$). The correlation to biomass species can be explained with emissions from biomass burning. Burning biomass can release inorganic aerosol constituents (calcium and potassium) and nitrogen species (ammonium and nitrate) (Savarino, et al., 1998). A massive area where biomass burning can occur is the high northern latitude, which would give rise to large amounts of mainly organic aerosols but also some inorganic aerosols in the Siberian forest. This could also explain the correlation between calcium and the biogenic species (Olivier, et al., 2006). Potassium shows its highest peak (133.6 ppm) in the summer of 2004.

MSA is analyzed in ice cores to investigate marine biogenic productivity. The only source for MSA is believed to be DMS. DMS is produced by marine phytoplankton found in high abundance in the Arctic Ocean. MSA is believed to be a potential sea-ice proxy, since the lowest concentrations of DMS are found under ice and the higher concentrations are found in open water near the ice margin (Isaksson, et al., 2005). The trendline of MSA shows an

increase in MSA concentration from 1984 to 2018 (Fig. 23.). A large increase can be seen between 2013 and 2016. If MSA can be used as a sea-ice proxy, the increased MSA concentration would indicate melting of ice in the Arctic Ocean. MSA also corroborates that transport from the Arctic Ocean to the Altai Mountains occurs. Since SO_2 is another oxidation product of DMS, a strong correlation between MSA and sulphate was expected. MSA correlated well with sulphate (r = 0.45), nitrate (r = 0.40) and potassium (r = 0.41). The correlation between MSA and potassium is not easily explained.

Fluoride originates from both natural and anthropogenic sources. The natural sources of fluoride in the atmosphere include volcanic eruptions, sea salt and dust particles. Aluminum smelters are one of the main anthropogenic sources of fluoride in the atmosphere. A by-product of aluminum smelters are the gases perfluorocarbons and hydrogen fluoride. Other anthropogenic sources are coal burning, industrial processing of cement and phosphate. The degradation of chlorofluorocarbons, which were widely used during the 20th century, can also affect the current fluoride concentrations (Preunkert, et al., 2001). Fluoride shows one large peak (32.9 ppm) at the beginning of 1994, while the average value for the measured fluoride concentration is 1.6 ppm (Fig. 23.). The cause of this fluoride peak is uncertain. Acetate shows two larger peaks, the first in 1994 and the second in 2014. Acetate does not correlate well with any other ion, which suggest contamination issues. The behaviour of acetate is unexpected and requires more strict quality control of the results because of contamination and chromatographic issues, this was not possible in the time frame of this thesis.

Some distinctive peaks for almost all the analyzed species can be seen for the years 1994, 2000, 2004, 2007 and 2014. This could be due to the common transport in the atmosphere or in some cases also due to enrichment in ice lenses. To determine which, further research is required.

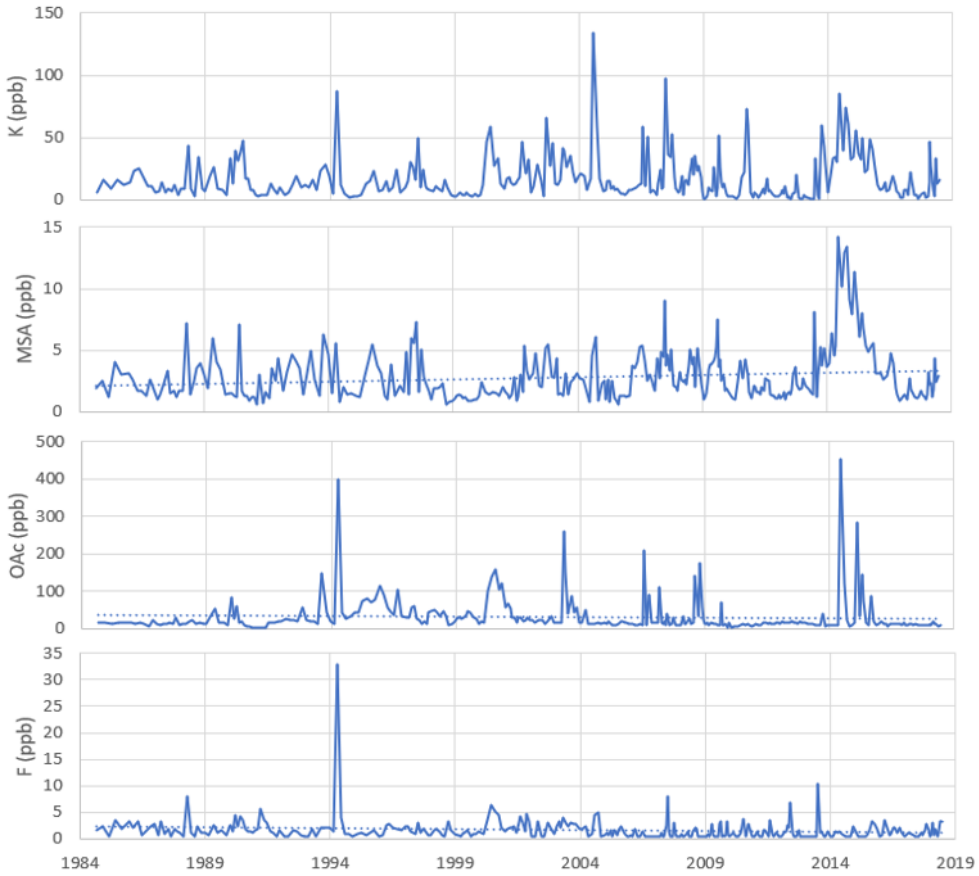

Fig. 23. Concentrations in ppb for the other analyzed species, potassium, MSA, acetate and fluoride.

6.5 Picarro results

6.5.1 $\delta^{18}O$

The $\delta^{18}O$ values show valuable information concerning the variations in the regional temperatures (Eichler et al., 2009a). The $\delta^{18}O$ values from the summer of 1985 to the summer of 2018 were obtained (Fig. 24.) Fluctuations are a result of isotopic fractionation. The values will be negative, since the ice cores contain a lower $^{18}O/^{16}O$ ratio than the water in the ocean. The $\delta^{18}O$ value during winter months will be more negative than the $\delta^{18}O$ value during summer. This is because the maximum amount of moisture in air decreases with decreasing temperature. The ice core will therefore show layers with both high and low $\delta^{18}O$ values. The extremely low value of -21.17‰ at year 2003 indicates a cold winter and the extremely high value of -9.64‰ at year 2018 indicates a warm summer. The $\delta^{18}O$ shows only a few strong winter minima and the average $\delta^{18}O$ value (-13.09‰) is relatively high considering the elevation (4506 m a.s.l.). This can be explained with the help of information received from the meteorological station Ak-kem (2000 m a.s.l.) located 7 km north of the Belukha glacier.

The precipitation at the Belukha glacier dominates during the summer months, i.e., June to August, with 58%. During the winter months, i.e. December to February, only 4% of the yearly precipitation is received (Eichler et al., 2009c). The average annual accumulation at Ak-kem can also be used to interpret the $\delta^{18}O$ results. This value for the years 1991 to 2000 at the Belukha glacier was calculated to be 0.42 m w.eq. and at Ak-kem 0.53 m w.eq. The lower value at the Belukha glacier is not to be expected, since the amount of precipitation should increase with increased altitude. The reason for the lower annual precipitation value at the Belukha glacier is most likely due to wind erosion. Some of the snow has been eroded with the wind, which decreases the amount of accumulation (Olivier, et al., 2019).

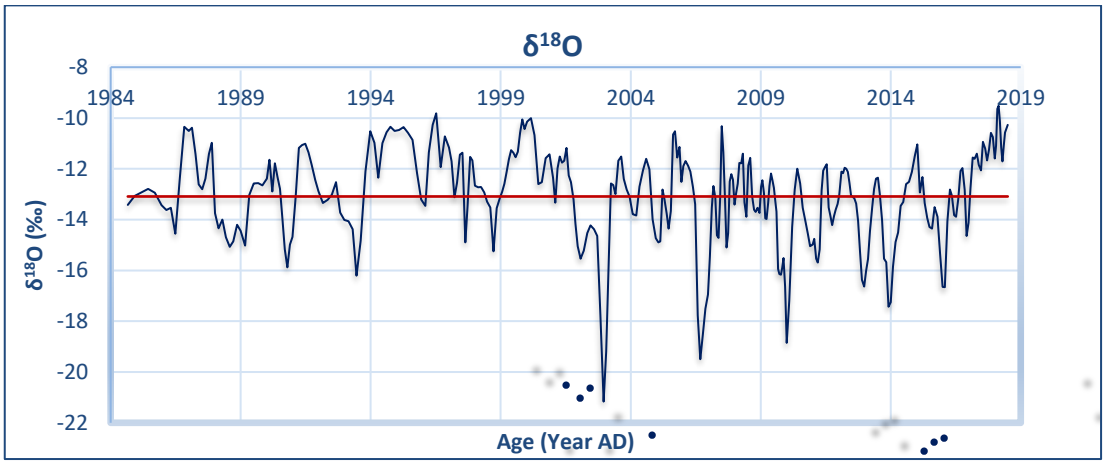

Fig. 24. $\delta^{18}O$ values are shown as a blue line and the mean value -13.09‰ is shown as a solid red line.

The $\delta^{18}O$ values for B01 and B18 are compared in Fig. 25. The values correlate well with each other. The only noticeable exception is at year 1987, where the value for B18 increased instead of decreased. This is most likely due to percolation of meltwater, which shifted the values. The annual average value for the years that exist in both ice cores, i.e. 1985 to 2000, are in excellent agreement. The annual average $\delta^{18}O$ value for this period for B01 is -12.66‰ and -12.45‰ for B18.

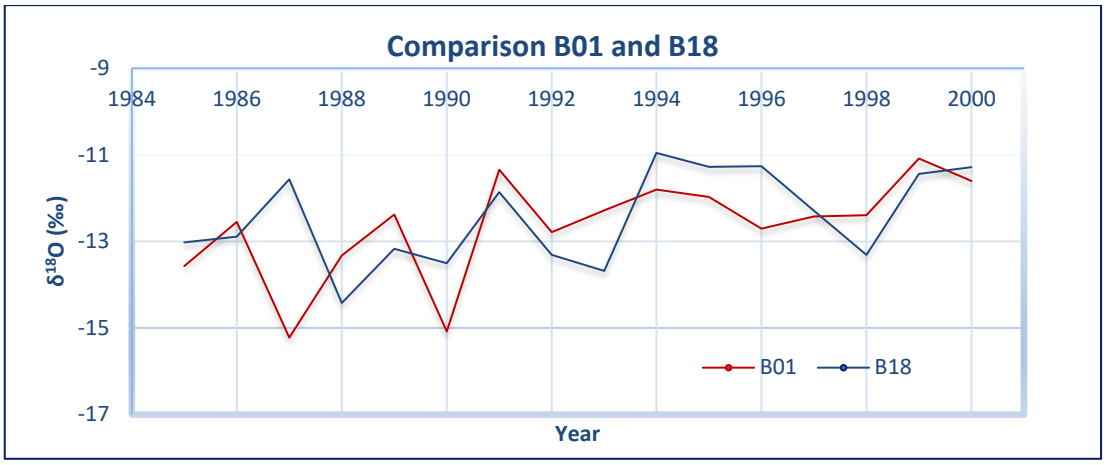

Fig. 25. Comparison of $\delta^{18}O$ values between B01 and B18. The values are given in per mil (‰).

6.5.2 d-excess

The deuterium excess shows valuable information of water vapor source region and transport. The average d-excess globally is ~10‰. The relative humidity at the water vapor source plays an important role. When the relative humidity at the ocean surface is low, light water isotopologues will preferably evaporate (kinetic effect) resulting in more depleted (negative) $\delta^{18}O$ values of water vapour, which increases the d-excess. This means that the d-excess will have a higher value during the winter months compared to the summer months (see Fig. 26.) (Bershaw, 2018). Another factor that increases the d-excess is the re-evaporated water vapor from internal sources, i.e. continental sources. The highest d-excess values can be seen during winter months, when the Siberian High restricts intrusion of air masses from external sources. This precipitation is brought by the southern cyclones from the Aral-Caspian Sea, the Mediterranean Sea and the Black Sea. Evaporation from plants and animals also increases the d-excess value. The lowest values can be seen during summer months, when the western cyclones bring precipitation from the Atlantic Ocean. Some summer precipitation can also originate from the Pacific Ocean and Arctic Ocean. The accumulation of both internal and external sources is higher during the summer months. The main amount of precipitation in the Siberian Altai originates from marine sources, with the Atlantic Ocean as the main source (Aizen, et al., 2006).

The average d-excess value of the analyzed part of B18 is 16.30‰. The highest value of 22.72‰ occurred during the winter of 2018 and the lowest value of 10.16‰ occurred during the summer of 2012. Negative anomalies in the d-excess record can be seen between 1987 and 1993. This is most likely due to changes in the moisture source, i.e. decreased amount of

re-evaporated precipitation or increase in oceanic precipitation. Positive anomalies can be seen between 1999 and 2006, with causes vice versa of the negative ones.

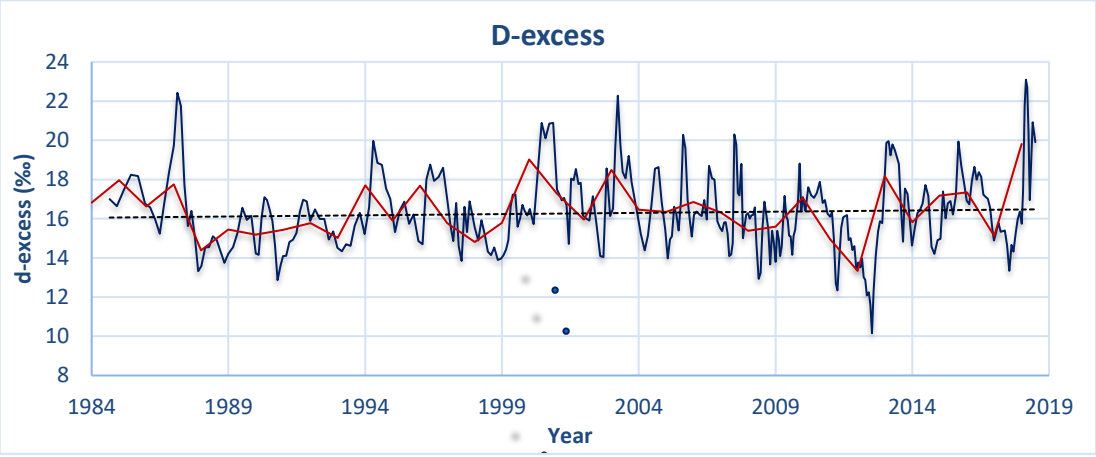

Fig. 26. d-excess values in ‰ from end of 1984 to the middle of 2018. The average annual values for d-excess are shown as a red line. The average d-excess value is shown as a black dotted line.

6.6 BC concentrations

The BC concentrations show two pronounced maxima, the first in the middle of 1992 (89.6 ppb) and the second at the end of 2004 (39.2 ppb) (Fig. 27.). At first glance, one might think that something went wrong in the analysis, since the values of these peaks are so much higher. With a closer inspection one can see that the peaks are formed by values from two analyzed samples (two dots), which indicates that the analysis is correct. The average value for all samples is 5.56 ppb. The red line shows the trendline of BC concentrations, which is steadily decreasing from 1984 towards 2018 (Fig. 27.). The year-to-year fluctuations can be explained with transport fluctuations, but the general downwards trend must be explained with something else. Generally, a 70% decrease of BC concentrations can be seen. At the end of the ice core (1984), the mean value was 10 ppb and at the beginning of the ice core (2018) the mean value was 3 ppb. This decrease can be attributed to the reduction of BC emissions after the dissolution of the USSR (Osmont, et al., 2018). Reduction in other anthropogenic sources could also contribute to the reduced rBC values, e.g. the mitigation policies for residential, industry and road transport emissions. The air quality can effectively be improved with emission mitigation policies.

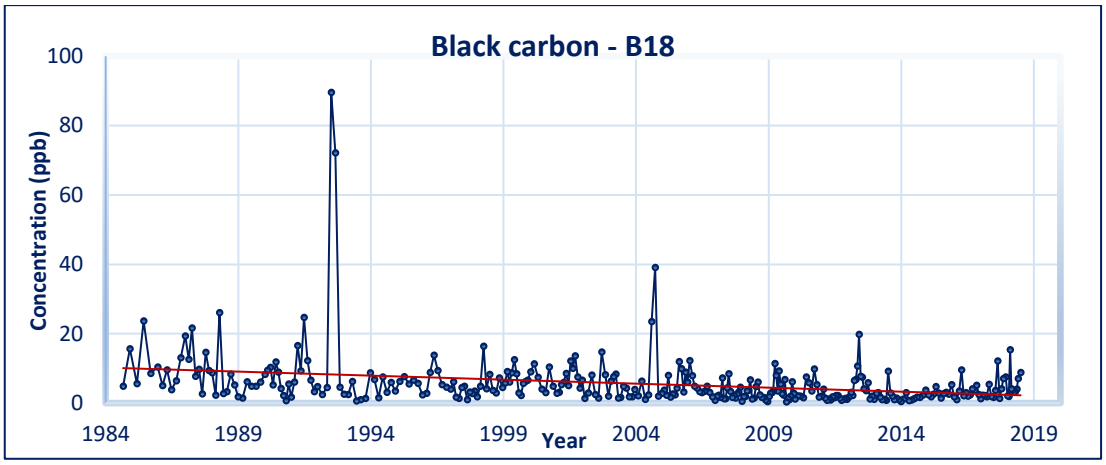

Fig. 27. BC data for B18 from 1984 to 2018. The average value is shown as a red line.

At Kevo (69°45'N, 27°02'E), in the Finnish Arctic, direct measurements of BC concentration have been made from 1964 to 2010. This was accomplished with filter samples. A general decrease in the BC concentration was seen at Kevo as well; the decrease was calculated to be ~1.8% yr^{-1} (Dutkiewicz, et al., 2014). The yearly decrease for the B18 ice core can also be calculated. The calculations did not include the years 1984 or 2018, since the data are not available for the entire year, which leads to a total period of 32 years (1985 to 2017). The average value for the first ten rBC samples (10.57 ppb) and the last ten rBC samples (4.70 ppb) was calculated (Equation 8.). The significant decrease rate was calculated at 1.7% yr^{-1}. This correlates well with the result from Kevo.

$$\frac{10.57\ ppb - 4.70\ ppb}{32\ yr\ x\ 10.57\ ppb}\ x\ 100 = 1.7\%\ yr^{-1}$$

Equation 8. The calculations for percent decreased concentration per year.

Most of the BC originates from anthropogenic sources, i.e. energy production, industry, diesel engines and residential biofuel uses. Until the mid-20th century, the Western countries were mainly responsible for the BC emissions. Currently, Asia with its emerging global economy is the major contributor. Natural sources, e.g. biomass burning, also affect the BC concentration, but on a much smaller scale (Osmont, et al., 2018). The rBC concentration was compared with NH_4^+ and $HCOO^-$ concentration to see if trends from biomass burning could be seen. For both rBC peaks a simultaneous increase in NH_4^+ and $HCOO^-$ was seen (Fig. 28.). To see if the peaks could be related to anthropogenic sources as well, comparison with SO_4^{2-} was performed. It is important to keep in mind that melting might have affected the concentration. The detailed source attribution for BC is difficult, since several emission sources exist. Since the anthropogenic emission sources are quite constant, it is believed that

the peaks in 1992 and 2004 are due to biomass burning. The peak in 1992 is not accompanied by a high sulfate peak, which indicates that the BC originates from biomass burning. The extra biomass burning could originate from natural sources, e.g. wildfires.

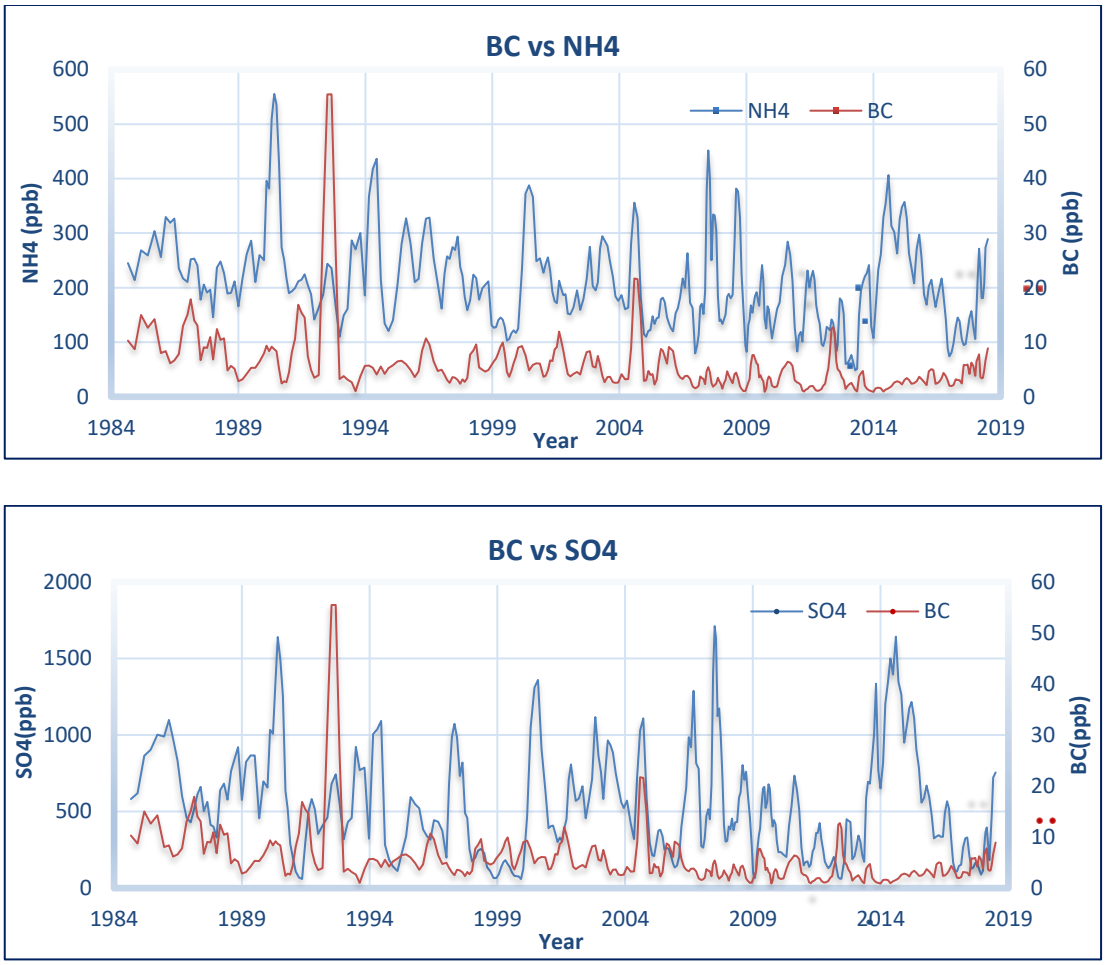

Fig. 28. The upper diagram is a comparison between BC and NH_4^+. The lower is a comparison between BC and SO_4^{2-}. Both diagrams are shown as 3-point moving average to smoothen the lines.

Since BC was not measured for B01, the B18 record will be compared with an ice core drilled from Tsambagarav (Fig. 4.). Tsambagarav (4130 m asl, 48°39.338'N, 90°50.826'E) is also a mountain peak in the Altai Mountain range, it is located in Western Mongolia (Herren, et al., 2013). There are two clear peaks in the BC data from Tsambagarav. The first one is in the spring of 1995 (69.7 ppb) and the second is in the summer of 2008 (31.0 ppb). This is very interesting, since both ice cores exhibits two peaks with almost the same concentration, but 3 to 4 years apart. The distance between Belukha and Tsambagarav is 325 km, but the peak difference cannot be explained by distance between the sites. The reason for the peak difference is, therefore, most likely due to dating uncertainty in both ice cores.

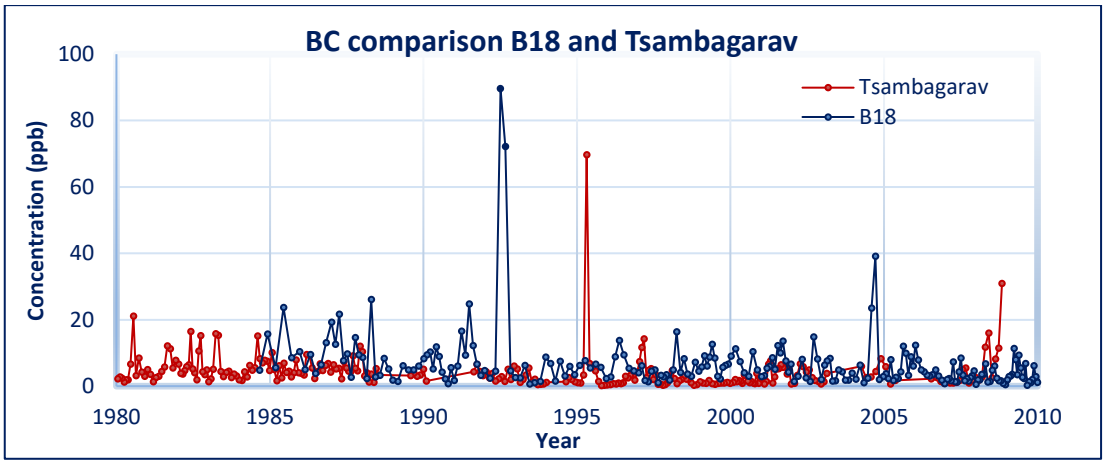

Fig. 29. BC data comparison between B18 and Tsambagarav.

7 SUMMARY AND CONCLUSIONS

The first 26.5 m of the B18 was successfully analyzed and dated at PSI. The samples needed for the major ion, stable isotope and BC analyses were cut into pieces with 8 cm resolution in a -20 °C cold room. The dating was performed with the help of the B01 ice core, and the concentrations were compared to each other to find overlapping concentration trends. The dust peak in B01 proved to be significant for the dating process. Thanks to this peak the year 2001 could be determined in the B18. The B01 was also used to determine the last year in B18. With the help of annual signals from ions and SWI, the rest of the years could be attributed. Some ice lenses were observed, which indicated surface melting on the glacier. This made the dating process more difficult, since some annual signals were shifted. The last year in this part of B18 was estimated to be 1983, this estimation was done with the help of the accumulation rate from B01 (0.56 m w.eq.). The final year of this analyzed part of B18 turned out to be the year 1984.7, which was very close to the first estimation.

In addition to ice lenses, other stratigraphic features of interest were also seen in the ice core. A 1.5 cm thick dust layer at a depth of 759.3 m w.eq. was seen as an orange layer in the ice core, corresponding to the beginning of 2006. An increase in the main dust-related species, namely calcium and magnesium, could be seen at the depth corresponding to the same time. The source for this dust is most likely from the arid region of central Asia. An overview of the dust-related species shows a decreasing trend from 1984 to 2018. This could possibly be due to fewer dust events at Belukha. Dust events are uncommon at Belukha, since only one dust layer could be visually noted in 34 years. Beside the dust particles, an insect was also observed in the ice core. This insect was found at a depth of 11.7 m w.eq., which corresponded to the summer of 1998. The insect was most likely a mosquito, but further analyzes on the mosquito was not conducted.

The accumulation rate for B18 was calculated to be 0.51 m w.eq., which is almost the same as the accumulation rate for B01. The comparison between the accumulation rate for Belukha and the meteorological station Ak-kem suggested some loss of precipitation at Belukha due to wind erosion. This did not come as a surprise since this was already shown for the B01. The mean $\delta^{18}O$ value for the analyzed part of B18 was -13.09‰, which is considered a high value for the elevation of 4506 m a.s.l., the mean value was high due to only a few strong winter minima. The lowest $\delta^{18}O$ value of -21.17‰ occurred in year 2003 and the highest $\delta^{18}O$ value of -9.64‰ occurred in year 2018. The annual $\delta^{18}O$ value for B01

and B18 are in excellent agreement for the time period 1985 to 2000. The annual average $\delta^{18}O$ value for this period for B01 is -12.66‰ and -12.45‰ for B18. The d-excess holds information of the water vapor source. The higher d-excess values originates mostly from re-evaporated water vapor from internal sources. Whereas the lower d-excess values originate from external sources. This means that the values will be higher during the winter months, when the air transport to the Altai mountains is restricted by the presence of the Siberian High.

The obtained information from the analyses was manifold. The ion impurity origin could be determined with the help of correlation analysis. Most of the analyzed ions could be assigned to one of the following groups: dust, anthropogenic or biomass related species. The expected fluctuation agreed well with the obtained results, i.e. an increase in concentration during the summer months. The lower concentration during the winter months is caused by restriction of convection due to vertical stability of the atmosphere and the presence of the Siberian High. Increased concentration trends for almost all analyzed species could be seen for the years 1994, 2000, 2004, 2007 and 2014. This is most likely due to enrichment in ice lenses or due to common atmospheric transport.

The sources for dust-related species were believed to be the deserts Kara-Kum, Kyzyl-Kum, Mojyn-Kum, Taklimakan and the Kazakh loess hills. An additional input of the sea salt-related species could not be neglected, the main origin was believed to be the evaporite deposits and water sources. Sodium and chloride could therefore have an additional source from the Aral Sea basin, the Atlantic Ocean and the seas in the Middle East. Ammonium correlated well with most of the analyzed ions, which suggested multiple sources. The anthropogenic sources were believed to be emissions from livestock wastes, fertilizers and bacterial decomposition and natural sources was believed to be biogenic and biomass burning emissions. Formate and ammonium had the third and fourth highest concentration in the analyzed part of B18, which suggest a significant input of biogenic emissions from Siberia. The large stored terrestrial carbon in Siberia might cause increased forest fire activity, if the estimated temperature increase in Asia occurs. The two highest ion concentration in the analyzed part of B18 were sulfate and nitrate. These secondary aerosols are produced by oxidation of SO_2 and NO_X, which mainly originates from anthropogenic sources, e.g. fossil-fuel burning, industrial and traffic emissions. The natural sources for these ions are, e.g. volcanic emissions, biomass burning and lightning.

MSA is believed to be a sea-ice proxy, and the increasing trend suggested melting of sea ice in the Arctic Ocean between 2013 to 2016. Potassium is the only other ion that showed an increasing trend from 1984 to 2018. The highest correlation for potassium is with calcium ($r = 0.71$). These ions have a common origin from inorganic aerosols from biomass burning emission. A decreasing trend is seen for calcium, but the largest share of calcium originates most likely from dust. One possibility is that the amount of calcium has decreased more than a possible increase of calcium from biomass burning. But the other biogenic and biomass burning related species, i.e. formate, oxalate and ammonium, shows a decreasing trend. Another possibility for the increased potassium concentration could be a change in dust sources. The dust could originate from a source with a higher concentration of potassium-based minerals. The ions with no visible change in concentration during this time period was nitrate and acetate.

The BC concentration also showed a significant decrease, due to cleaner cars and fewer coal fired power plants. The decrease rate for BC at Belukha was calculated to be 1.7% yr^{-1}. The main part of the BC particles was believed to originate from anthropogenic sources, e.g. energy production and industry, and the natural sources, e.g. biomass burning, was believed to be less significant. A decrease in concentration can also be seen for sulfate but not for nitrate. NO_x emissions could still be high due to the increased number of cars and higher emissions than anticipated. The BC concentration was not measured for the B01. The B18 BC concentration was, therefore, compared with a BC record from an ice core obtained from Tsambagarav. The two distinctive BC concentration peaks could be seen in both ice cores, but with a few years apart. This was most likely due to dating uncertainty in both ice cores, but further research is needed. At its deepest point, the B18 dates around 20000 years back in time.

8 ACKNOWLEDGEMENTS

This thesis is performed as a collaboration between the analytical chemistry department at Åbo Akademi University in Finland and the Laboratory of Environmental Chemistry at Paul Scherrer Institute (PSI) in Switzerland. First, I want to thank all three of my supervisors. I want to thank Prof. Dr. Margit Schwikowski-Gigar for offering me an internship position at PSI. I also want to thank both of my supervisors at Åbo Akademi University, Assoc. Prof. Tom Lindfors and Dr. Rose-Marie Latonen, for taking on the responsibility of a supervisor role, even if paleoclimatology research is not their area of expertise. I would also like to thank my supervisors for their guidance and support during this process. I am grateful for the open communication and understanding between all parties involved. Thanks to this cooperation, it was possible for me to conduct the laboratory work required for my master's thesis at PSI.

Secondly, I would like to thank the people who I worked with at PSI. I want to thank the PhD students Petr Nalivaika and Thomas Singer for teaching me how to work in the cold room, helping with the data analysis, but also for showing me around and helping out on a daily basis. A special thanks to Dr. Anja Eichler for always being willing to lend a helping hand. I want to thank Sabina Brütsch for teaching me how to work with the analysis instruments in the lab, but also for all the German she taught me. I want to thank all the people at PSI who made me feel welcome and part of their research group. I am grateful for the new friendships that I made at the PSI Guest House and for all the wonderful memories we created together. Lastly, I would like to thank my family and friends for the support.

"The farther backward you can look, the farther forward you are likely to see."

- Winston Churchill

9 SUMMARY IN SWEDISH – SVENSK SAMMANFATTNING

Den här magisteravhandlingen utfördes som ett samarbete mellan Åbo Akademi och Paul Scherrer Institute. Den svenska titeln för avhandlingen är ”En analys av främsta joner, stabila vattenisotoper samt svarta kolpartiklar i den övre delen av Belukha iskärnan från Sibiriska Altai”.

Glaciärer innehåller information om kemiska föroreningar och stabila vattenisotoper. De fungerar därför som naturliga arkiv för tidigare klimat och luftföroreningar. Denna information är välbevarad om smältning försummas samt om den årliga nederbörden förekommer som snö. Den hydrologiska cykeln och fördelningen av stabila vattenisotoper mellan de olika reservoarerna kan användas för att förutspå tidigare temperaturer. Då vattnet förflyttar sig i den hydrologiska cykeln kommer ^{16}O-isotoper att anrikas, eftersom ^{18}O-isotoperna är tyngre. Den här fraktioneringen är temperaturberoende och förhållandet mellan $^{18}O/^{16}O$-isotoper ($\delta^{18}O$) kan därför användas för att bestämma variationer i tidigare temperaturer. Depositionen av kemiska föroreningar är störst under sommaren, eftersom lufttransporten förhindras av de torra och kalla förhållandena under vintern. För tillfället minskar volymen av glaciärer runtom i världen och det är därför viktigt att bedriva paleoklimatologisk forskning samt bevara iskärnor medan möjligheten fortfarande finns.

För den aktuella studien skars iskärnorna enligt tidigare utförda beräkningar och skärningsscheman i ett kylrum med -20 °C. För att minimera kontamineringsrisken är det av yttersta vikt att kylrummet är rent. Största delen av de observerade islinserna var under 3 cm, islinser återger mängden smältning på glaciären. Det bör beaktas att smältvattnets perkolering kan störa de årliga kemiska signalerna. Därefter kunde proven analyseras med IC, WS-CRDIS och SP2. Det finns flera olika tillvägagångssätt för datering av iskärnor. Vanligtvis används stratiografiska markörer, radioaktivt sönderfall och säsongsvarierande signaler. Dateringen för denna iskärna utfördes genom att jämföra de kemiska signalerna med en annan iskärna som borrades från Belukha-glaciären år 2001. En distinkt topp av dammrelaterade joner och säsongsvarierande signaler visade sig vara betydelsefull för datering. Iskärnan sträckte sig tillbaka till 1984 och de kemiska signalerna stämde generellt bra överens mellan de två iskärnorna från Belukha.

Sammanlagt analyserades tretton olika joner och genom att beräkna korrelationskoefficienten mellan jonerna kunde slutsatser om gemensamt ursprung

konstateras. Calcium, magnesium, natrium och klorid hörde till dammrelaterade partiklar, med ursprung från öknar, och ytterligare källa för natrium och klorid var havssalt. Nitrat, sulfat och ammonium hörde till de antropogent-relaterade partiklar, med ursprung från trafikutsläpp, förbränning av fossila bränslen och gödsel. Ammonium hörde även, tillsammans med format och oxalat, till partiklar som var relaterade till biogena arter och biomassa. Största delen av dessa partiklar kommer från Sibirien, som är en av de största reservoarerna av terrestrialt kol i världen. Övriga analyserade joner var fluorid, MSA, acetat och kalium. MSA tros vara en potentiell havsis-proxy och visade ökad havsissmältning 2013 – 2016. För acetat och kalium fanns flera potentiella ursprung. Nästan alla joner uppvisade en minskande trend i koncentrationen från 1984 – 2018.

Det genomsnittliga $\delta^{18}O$-värdet (-13,09‰) var relativt högt med tanke på elevationen (4506 m ö.h.), vilket indikerar en brist på starka vinterminima. Det lägsta uppmätta värdet (-21,17‰) år 2003 indikerar den kallaste perioden och det högsta uppmätta värdet (-9,64‰) år 2018 indikerar den varmaste perioden. Trenden för den årliga Den $\delta^{18}O$-koncentrationen för de två iskärnorna uppvisade endast en märkbar avvikelse, vilket högst antagligen beror på smältvattenperkolation. Deuteriumöverskottet var högre under vintermånaderna och lägre under sommarmånaderna, vilket tyder på en tillförsel av vattenånga från interna källor under vintern och från externa källor under sommaren. Den största andelen av nederbörden i Sibiriska Altai kommer från marina källor, med Atlanten som huvudkälla. Andra källor till nederbörd är till exempel Medelhavet samt avdunstning från växter och djur. Den genomsnittliga årliga ackumuleringsgraden var 0,51 m vattenekvivalent.

Svarta kolpartiklar bildas vid ofullständig förbränning av kolhaltigt material, dvs. biomassa och fossilt bränsle. De unika egenskaperna hos svarta kolpartiklar, dvs. den låga kemiska aktiviteten, den stora ljusabsorberingsförmågan samt den höga eldfastheten, påverkar jordens strålningsbudget. Dessa partiklar bidrar till den globala uppvärmningen genom att reducera albedoeffekten, direkt absorbera solljus i atmosfären samt genom att modifiera molnegenskaper. Analysen av de svarta kolpartiklarna visade två distinkta toppar. Koncentrationen av de svarta kolpartiklarna jämfördes med en iskärna från Tsambagarav, som befinner sig 325 km från Bleukha. De två distinkta topparna kunde även ses i Tsambagaraviskärnan men 3–4 år senare än i Belukha. Detta beror troligtvis på dateringsosäkerheter.

10 REFERENCES

Aizen, V. B., Aizen, E. M., Joswiak, D. R., Fujita, K., Takeuchi, N., & Nikitin, S. A. (**2006**). *Climatic and atmospheric circulation pattern variability from ice-core isotope/geochemistry records (Altai, Tien Shan and Tibet)*. Ann. Glaciol., *43*(1).

Baumgardner, D., Kok, G., & Raga, G. (**2004**). *Warming of the Arctic lower stratosphere by light absorbing particles*. Geophys. Res. Lett., *31*(1).

Berden, G., Peeters, R., & Meijer, G. (**2000**). *Cavity ring-down spectroscopy: Experimental schemes and applications.* Rev. Phys. Chem., *19*(4).

Beria, H., Larsen, J. R., Ceperley, N. C., Michelon, A., Vebbemann, T., & Schaefli, B. (**2018**). *Understanding snow hydrological processes through the lens of stable water isotopes*. WILEY, *5*(6).

Bershaw, J. (**2018**). *Controls on Deuterium Excess across Asia*. Geosci., *8*(7).

Bronex, J., Gagliardini, O., Gillet-Chaulet, F., & Chekki, M. (**2020**). *Comparing the long-term fate of a snow cave and a rigid container buried Dome C, Antarctica*. Reg. Sci. Technol., *180*.

Dutkiewicz, V. A., DeJulio, A. M., Ahmed, T., Laing, J., Hopke, P. K., Skeie, R. B., Viisanen, Y., Paatero, J., Husain, L. (**2014**). *Forty-seven years of weekly atmosphericblack carbon measurements in the FinnishArctic: Decrease in black carbonwith declining emissions*. Geophys. Res. Atmos., *119*(12).

Eichler, A., Schwikowski, M., Gäggeler, H. W., Furrer, V., Synai, H.-A., Beer, J., Matthias, S., Funk, M. (**2000**). *Glaciochemical dating of an ice core from upper Grenzgletscher (4200 m a.s.l.)*. J. Glaciol., *46*(154).

Eichler, A., Olivier, S., Henderson, K., Laube, A., Beer, J., Papina, T., & Gäggeler, H. W. (**2009a**). *Temperature response in the Altai region lags solar forcing*. Geophys. Res. Lett.,*36*(1).

Eichler, A. B., Olivier, S., Papina, T., & Schwikowski, M. (**2009b**). *A 750 year ice core record of past biogenic emissions from Siberian*. Geophys. Res. Lett., *36*(18).

Eichler, A., Olivier, S., Henderson, K., Laube, A., Beer, J., Gäggeler, H. W., & Papina, T. S. (**2009c**). *Temperature Changes in the Altai Are Driven by Solar and Anthropogenic Forcing*. Geophys. Res. Lett., *63*(12).

Fang, L., Jenk, T. M., Singer, T., Hou, S., & Schwikowski, M. (**2021**). *Radiocarbon dating of alpine ice cores with the dissolved organic carbon (DOC) fraction*. The Cryosphere, *15*(3).

Gäggeler, H. W., Tobler, L., Schwikowski, M., & Jenk, T. (**2020**). *Application of the radionuclide 210Pb in glaciology - an overview*. J. Glaciol., *66*(257).

Gäggeler, H., Gunten, H. R., Rössler, E., Oeschger, H., & Schotterer, U. (**2017**). *210Pb-Dating of Cold Alpine Firn/Ice Cores From Colle Gnifetti, Switzerland*. J. Glaciol. *29*(101).

Gao, R. S., Schwarz, J. P., Kelly, K. K., Fahey, D. W., Watts, L. A., Thompson, T. L., Spackman, J. R., Slowik, J. G., Cross, E. S., Han, J.-H., Davidovits, P., Onasch, T. B., Worsnop, D. R. (**2007**). *A Novel Method for Estimating Light-Scattering Properties of Soot Aerosols Using a Modified Single-Particle Soot Photometer*. Aerosol Sci. Technol., *41*(2).

Gao, R. S.; Schwarz, J. P.; Kelly, K. K.; Fahey, D. W.; Watts, L. A.; Thompson, T. L.; Spackman, J. R.; Slowik, J. G.; Cross, E. S.; Han, J. -H.; Davidovits, P.; Onasch, T. B.; Worsnop, D. R.

Garzonio, R., Di Mauro, B., Strigaro, D., Rossini, M., Colombo, R., De Amicis, M., & Maggi, V. (**2017**). *Mapping the suitability for ice-core drilling of glaciers in the European Alps and the Asian High Mountains*. J. Glaciol., *64*(243).

Grigholm, B., Mayewski, P., Azien, V., Kreutz, K., C.P., W., Azien, E., Kang, S., Maasch, K. A., Handley, M. J., Sneed, S. (**2016**). Mid-twentieth century increase in anthropogenic Pb, Cd and Cu in central Asia set in hemispheric perspective using Tien Shan ice core. Atmos. Environ*., 131*.

Gusev, A. (**2009**). *Heavy metals emission to air*. *HELCOM Indicator Fact Sheets 2009. Online. [08.02.2020], http://www.helcom.fi/environment2/ifs/en_GB/cover/*.

Haddad, P. R., & Jackson, P. E. (**1990**). *Ion Chromatography principles and application.* Elsevier Science B.V. (Book).

Henderson, K., Laube, A., Gäggeler, H. W., Olivier, S., Papina, T., & Schwikowski, M. (**2006**). *Temporal variations of accumulation and temperature during the past two centuries from Belukha ice core, Siberian Altai*. J. Glaciol. Res., *111*.

Herren, P.-A., Eichler, A., Machguth, H., Papina, T., Tobler, L., Zapf, A., & Schwikowski, M. (**2013**). *The onset of Neoglaciation 6000 years ago in western Mongolia revealed by an ice core from the Tsambagarav mountain range*. Quat. Sci. Rev., *69*.

Ice Memory. **2020**, accessed 2 of May 2021, <https://www.ice-memory.org/en/>.

IPCC, **2001**: Folland, C.K., T.R. Karl, J.R. Christy, R.A. Clarke, G.V. Gruza, J. Jouzel, M.E. Mann, J. Oerlemans, M.J. Salinger and S.-W. Wang *Observed Climate Variability and Change. In: Climate Change 2001: The Scientific Basis. Contribution of Working Group I to the Third Assessment Report of the Intergovernmental Panel on Climate Change* [Houghton, J.T., Y.

IPCC, **2014**: *Climate Change 2014: Impacts, Adaptation, and Vulnerability. Summaries, Frequently Asked Questions, and Cross-Chapter Boxes. A Contribution of Working Group II to the Fifth Assessment Report of the Intergovernmental Panel on Climate Change* [Field, C.B., V.R. Barros, D.J. Dokken, K.J. Mach, M.D. Mastrandrea, T.E. Bilir, M. Chatterjee, K.L. Ebi, Y.O. Estrada, R.C. Genova, B. Girma, E.S. Kissel, A.N. Levy, S. MacCracken,P.R. Mastrandrea, and L.L. White (eds.)]. World Meteorological Organization, Geneva, Switzerland, 190 pp. (in Arabic, Chinese, English, French, Russian, and Spanish)

IPCC, **2019**: Hock, R., G. Rasul, C. Adler, B. Cáceres, S. Gruber, Y. Hirabayashi, M. Jackson, A. Kääb, S. Kang, S. Kutuzov, Al. Milner, U. Molau, S. Morin, B. Orlove, and H. Steltzer, 2019*: High Mountain Areas. In: IPCC Special Report on the Ocean and Cryosphere in a Changing Climate* [H.-O. Pörtner, D.C. Roberts, V. Masson-Delmotte, P. Zhai, M. Tignor, E. Poloczanska, K. Mintenbeck, A. Alegría, M. Nicolai, A. Okem, J. Petzold, B. Rama, N.M. Weyer (eds.)]. In press.

Isaksson, E., Kekonen, T., Moore, J., & Mulvaney, R. (**2005**). *The methanesulfonic acid (MSA) record in a Svalbard ice core*. Ann. Glaciol., *42*.

Klinge, M., Böhner, J., & Lehmkuhl, F. (**2003**). *Climate pattern, snow- and timberlines in the Altai Mountains, Central Asia*. Erdkunde, *57*(4).

Landais, A., Barkan, E., & Luz, B. (**2008**). *Record of d18O and 17O-excess in ice from Vostok Antarctica during the last 150,000 years*. Geophys. Res. Lett. *35*(2).

Malygina, N., Papina, T., Kononova, N., & Balyaeva, T. (**2017**). *Influence of atmospheric circulation on precipitation in Altai Mountains*. J. Mt. Sci., *14*(1).

Olivier, S., Blaser, C., Brütsch, S. F., W., G. H., Henderson, K. A., Palmer, A. S., Papina, T., Schwikowski, M. (**2006**). *Temporal variations of mineral dust, biogenic tracers, and anthropogenic species during the past two centuries from Belukha ice core, Siberian Altai*. Geophys. Res. Lett., *111*(5).

Olivier, S., Schwikowski, M., Brütsch, S., Eyrikh, S., Gäggler, H. W., Lüthi, M., Papina, T., Saurer, M., Schotterer, U., Tobler, L., Vogel, E. (**2019**). *Glaciochemical investigation of an ice core from Belukha glacier,Siberian Alta.* Geophys. Res. Lett., *30*(19).

Osmont, D., Wendl, I. A., Schmidely, l., Sigl, M., Vega, C. P., Isaksson, E., & Schwikowski, M. (**2018**). *An 800-year high-resolution black carbon ice core record from Lomonosovfonna, Svalbard*. Atmos. Chem. Phys., *18*(17).

Petzold, A., Ogren, J. A., Fiebig, M., Laj, P., Ll, S.-M., Baltensperger, U., Holzer-Popp, T., Kinne, S., Pappalardo, G., Sugimoto, N., Wehrli, C., Wiedensholer, A., Zhang, X.-Y. (**2013**). *Recommendations for reporting "black carbon" measurements.* Atmos. Chem. Phys., *13*.

Picarro. (**2021**). accessd 2 of May 2021, <https://www.picarro.com/company/technology/crds>.

Preunkert, S., & Legrand, M. (**2001**). *Causes of enhanced fluoride levels in Alpine ice cores over the last 75 years: Implications for the atmospheric fluoride budget*. J. Geophys. Res., *106*(12).

Rapp, D. (**2012**). *Ice Ages and interglacials* (Vol. 2). Berlin Heidelberg: Springer-Verlag (Book).

Savarino, J., & Legrand, M. (**1998**). *High northern latitude forest fires and vegetation emissions over the last millennium inferred from the chemistry of a central Greenland ice core*. J. Geophys. Res., *103*(D7).

Schwikowski, M., & Eichler, A. (**2010**). *Alpine Glaciers as Archives of Atmospheric Deposition. In Alpine Waters. The Handbook of Environmental Chemistry* (Vol. 6). Berlin, Heidelberg.: Springer (Book).

Schwikowski, M., Döscher, A., Gäggeler, H. W., & Schotterer, U. (**1999**). *Anthropogenic versus natural sources of atmospheric sulphate from an Alpine ice core*. Tellus B. *51*(5).

Sun, J., Zhang, M., & Liu, T. (**2001**). *Spatial and temporal characteristics of dust storms in China and its surrounding regions, 1960-1999: Relations to source area and climate*. J. Geophys. Res., *106*(10).

Sun, J., Birmili, W., Hermann, M., Tuch, T., Weinhold, K., Merkel, M., Rasch, F., Müller, T., Schladitz, A., Bastian, S., Löschau, G., Cyrys, J., Gu, J., Flentje, H., Briel, B., Asbach, C., Kaminski, H., Ries, L., Sohmer, R., Gerwig, H., Wirtz, K. (**2020**). *Decreasing trends of particle number and black carbon mass concentrations at 16 observational sotes in Germany from 2009 to 2018*. Atmos. Chem. Phys., *20*(11).

Voosen, P. (**2017**). *Record-shattering 2.7 million-year-old ice core reveals start of the ice ages*. Sci., *357*(6352).

11 APPENDICES

Appendix A – Remeasured major ion samples

Table 8. The IC values and limits for formate before and after the dilution.

IC sample	$HCOO^-$ limit (ppb)	$HCOO^-$ value (ppb)	Diluted $HCOO^-$ limit (ppb)	Diluted $HCOO^-$ value (ppb)
44	800	858.17	1600	858.24
50	800	1225.27	1600	1233.59
182	800	969.30	1600	969.30
220	800	1037.51	1600	1037.51
270	800	1038.87	1600	1038.87
274	800	838.84	1600	838.84
298	800	839.86	1600	769.24
299	800	985.94	1600	877.75
300	800	875.65	1600	786.90
327	800	896.25	1600	896.10

Table 9. The IC values and limits for sulfate before and after the dilution.

IC sample	SO_4^{2-} limit (ppb)	SO_4^{2-} value (ppb)	Diluted SO_4^{2-} limit (ppb)	Diluted SO_4^{2-} value (ppb)
50	2000	2093.30	4000	2128.21
270	2000	2498.99	4000	2498.96
297	2000	2205.86	4000	2225.72

Appendix B – Annual accumulation rate B18

Year	Depth (m w.eq.)	Annual accumulation (m w.eq.)
2018.5	0.00	-
2018	0.37	-
2017	0.86	0.49
2016	1.46	0.59
2015	2.01	0.56
2014	2.48	0.46
2013	3.00	0.53
2012	3.57	0.57
2011	4.21	0.63
2010	4.69	0.48
2009	5.54	0.86
2008	6.34	0.80
2007	7.16	0.82
2006	7.71	0.55
2005	8.40	0.70
2004	8.84	0.44
2003	9.41	0.57
2002	9.83	0.42
2001	10.48	0.65
2000	10.90	0.42
1999	11.54	0.64
1998	11.99	0.45
1997	12.55	0.56
1996	12.91	0.36
1995	13.22	0.30
1994	13.59	0.37
1993	13.90	0.32
1992	14.21	0.31
1991	14.66	0.45
1990	15.22	0.56
1989	15.56	0.34
1988	15.97	0.41
1987	16.45	0.49
1986	16.82	0.36
1985	17.06	0.24
1984.7	17.10	-

Appendix C – Ion comparison for B01 and B18

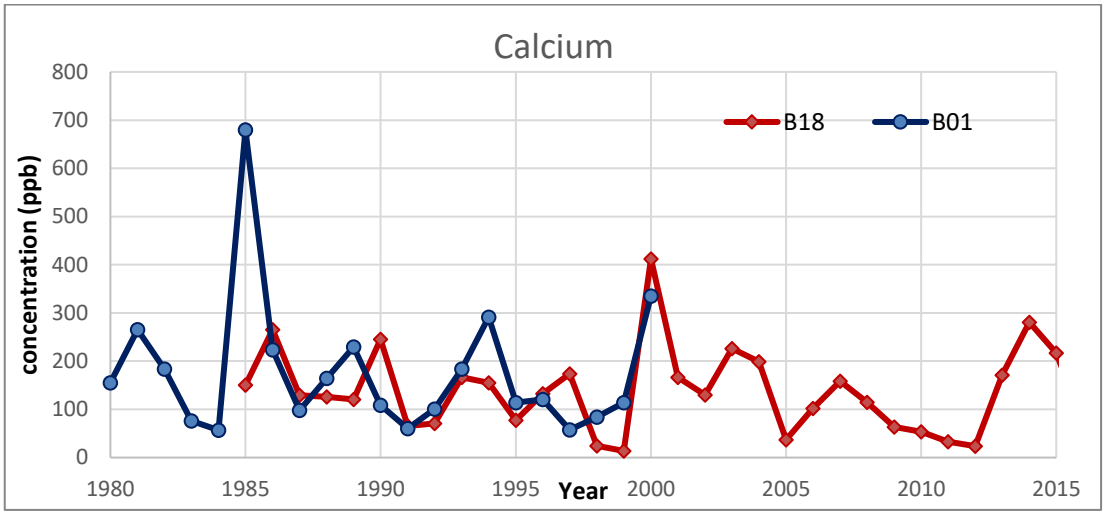

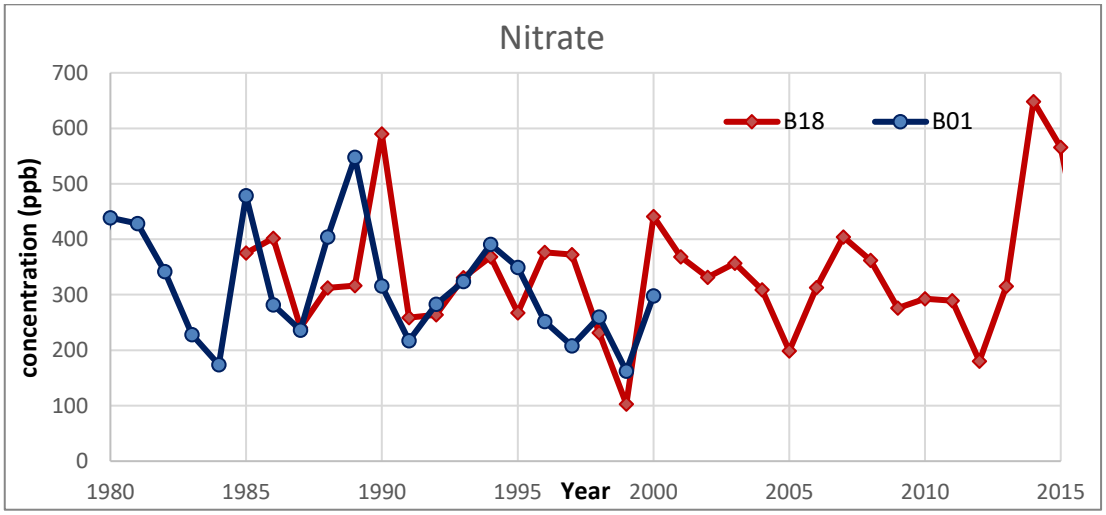

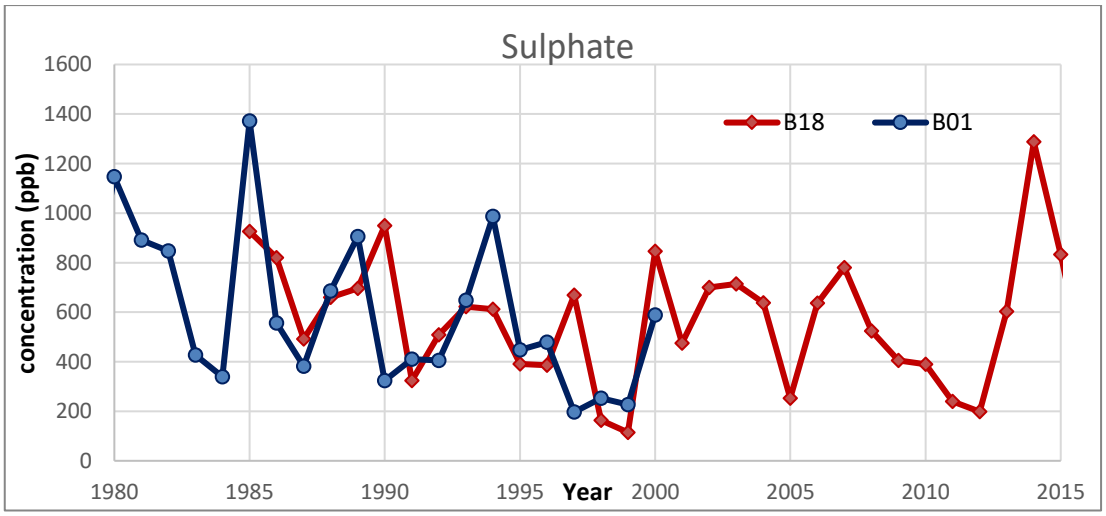

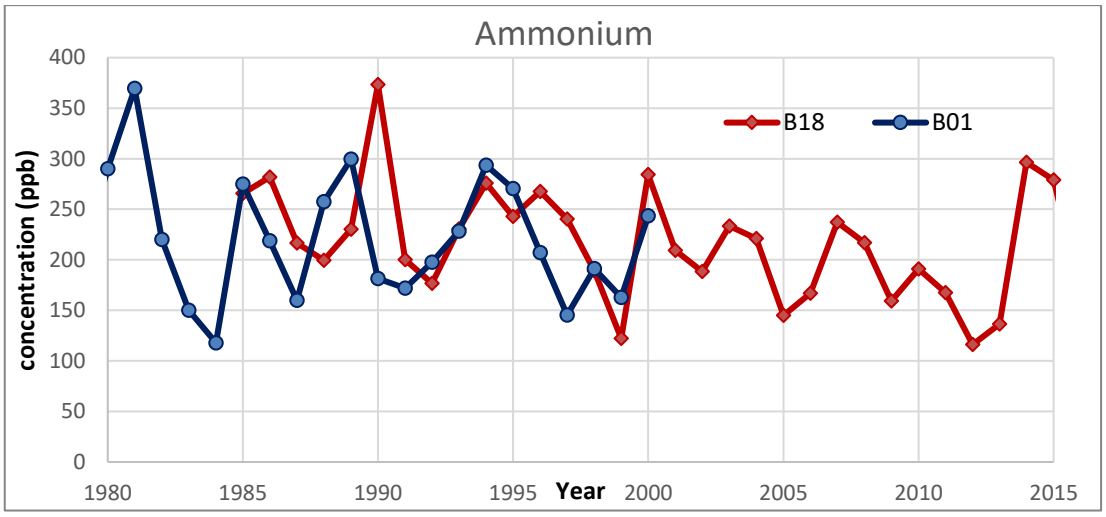
Ammonium
concentration (ppb)
400
350
300
250
200
150
100
50
0
1980
1985
1990
1995
Year
2000
2005
2010
2015
B18
B01

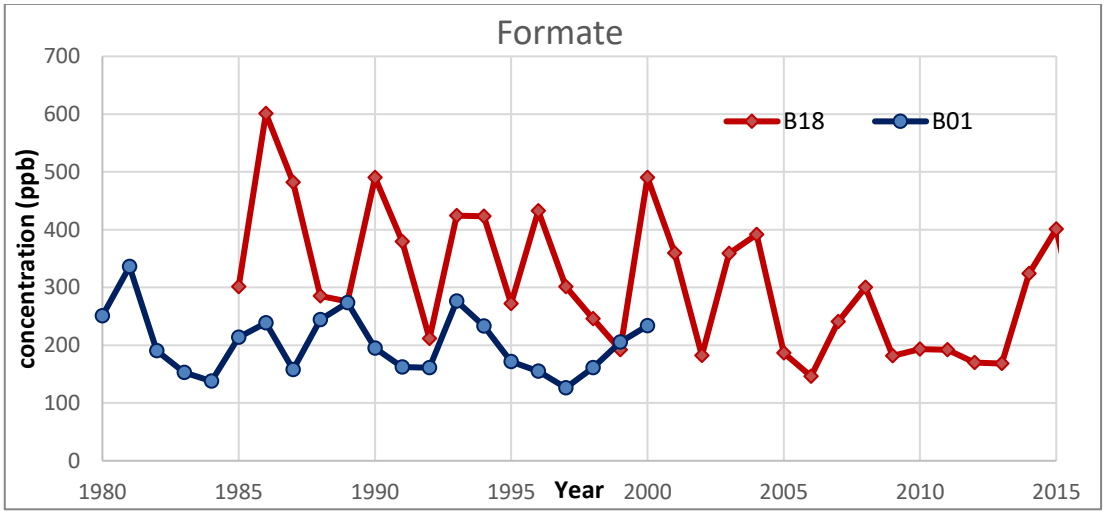
Formate
concentration (ppb)
700
600
500
400
300
200
100
0
1980
1985
1990
1995
Year
2000
2005
2010
2015
B18
B01

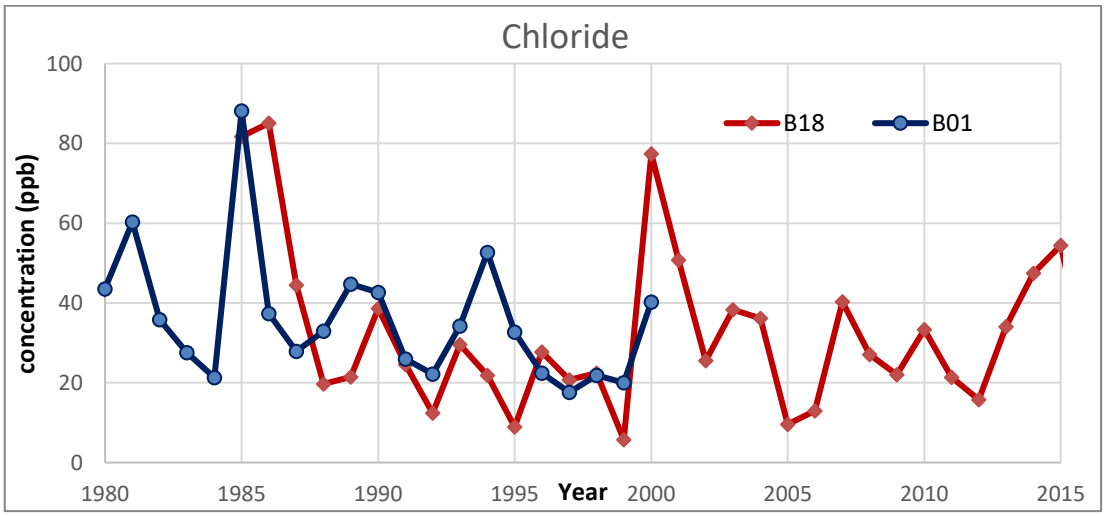
Chloride
concentration (ppb)
100
80
60
40
20
0
1980
1985
1990
1995
Year
2000
2005
2010
2015
B18
B01

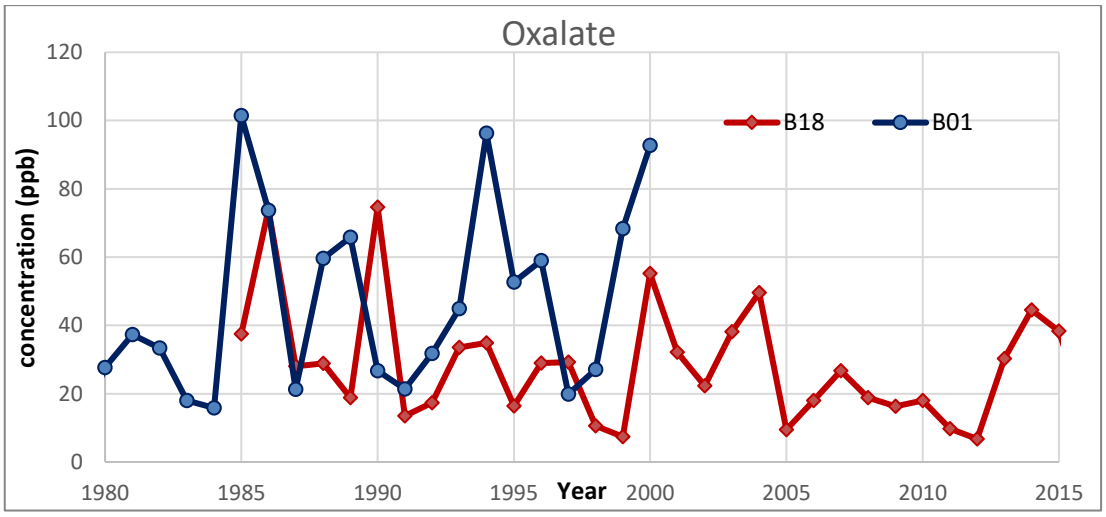
Oxalate
concentration (ppb)
120
100
80
60
40
20
0
1980
1985
1990
1995
Year
2000
2005
2010
2015
B18
B01

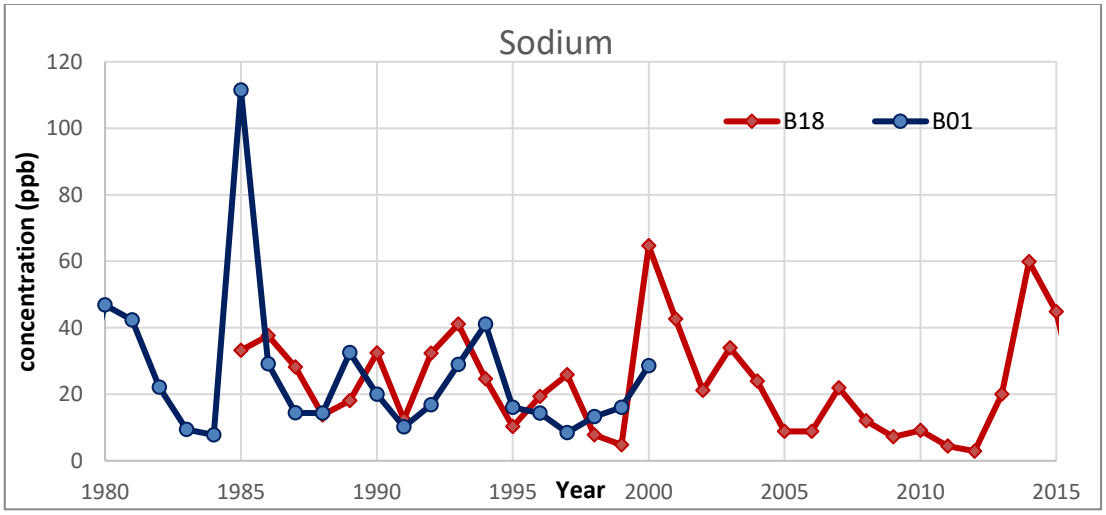
Sodium
concentration (ppb)
120
100
80
60
40
20
0
1980
1985
1990
1995
Year
2000
2005
2010
2015
B18
B01

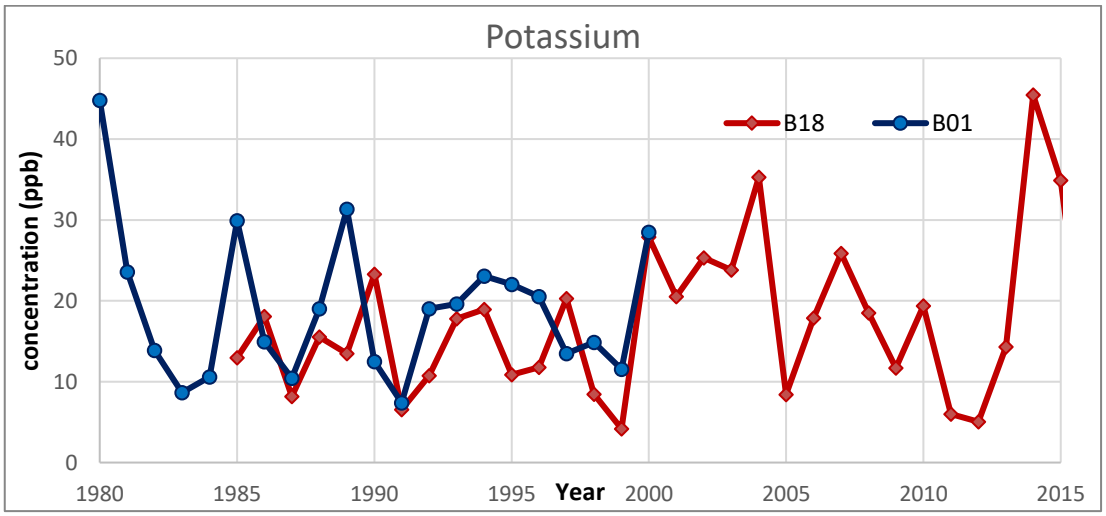
Potassium
concentration (ppb)
50
40
30
20
10
0
1980
1985
1990
1995
Year
2000
2005
2010
2015
B18
B01

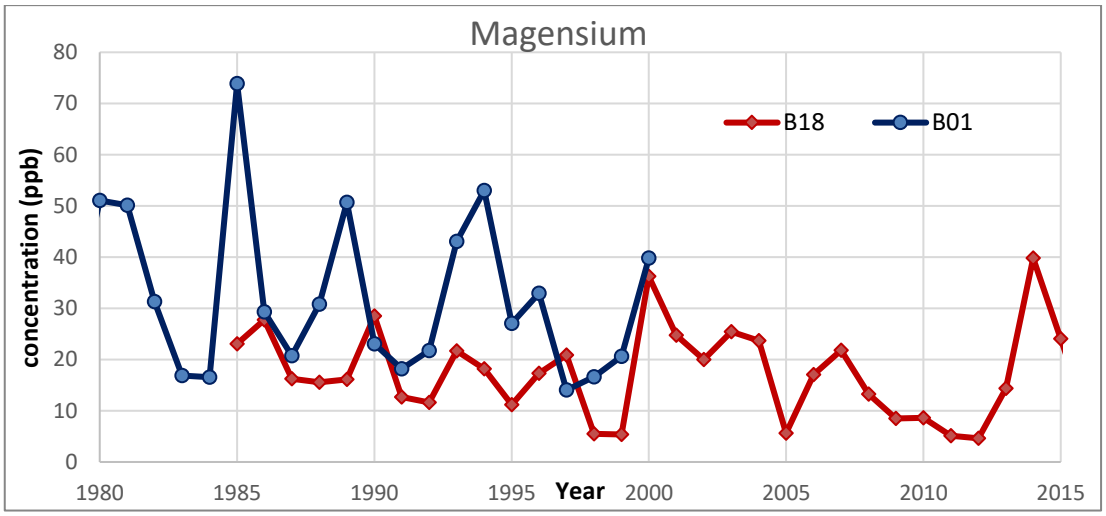
Magensium
B18
B01
concentration (ppb)
Year
0
10
20
30
40
50
60
70
80
1980
1985
1990
1995
2000
2005
2010
2015